Comparison of numerical modelling techniques for impact investigation on a wind turbine blade

Amrit Shankar Verma[a,b,*], Nils Petter Vedvik[c], Philipp Ulrich Haselbach[d], Zhen Gao[a,b], Zhiyu Jiang[b,e]

[a] *Department of Marine Technology, Norwegian University of Science and Technology, Norway*
[b] *Centre for Marine Operations in Virtual Environments (SFI MOVE), NTNU, Norway*
[c] *Department of Mechanical and Industrial Engineering, Norwegian University of Science and Technology, Norway*
[d] *Department of Wind Energy, Technical University of Denmark, Denmark*
[e] *Department of Engineering Sciences, University of Adger, 4879 Grimstad, Norway*

Abstract

Wind turbine blades are exposed to numerous impact risks throughout their lifetimes. The impact risks range from bird collisions during operation to impacts with surrounding structures at the time of transportation and installation. Impact loads on the fibre composite blades can induce several complex, simultaneously interacting and visually undetectable damage modes and have a high potential to reduce the local and global blade stiffness. An assessment of such impact-induced damages is therefore necessary and usually involves high computational costs using numerical procedures, especially when analysing large composite components. To minimise this computational expense, different numerical impact modelling techniques are utilised, primarily shell-element-based approaches and multiscale-modelling-based global-local approaches. In this article, a comparison between (1) pure shell, (2) shell-to-solid coupling, and (3) submodelling finite element modelling techniques using Abaqus/Explicit is presented for a case where an impactor hits the leading edge of a blade. A high-fidelity local solid finite element model is developed for the leading edge of a DTU 10 MW blade at the region of impact and its stiffness is compared with baseline. A user material subroutine VUMAT for the intralaminar damage mode based on the Hashin failure criterion is formulated and then validated via an experiment from the literature. Finally, based on different numerical modelling techniques, impact investigations are performed, and the impact responses, damage to the blade and computational analysis durations are compared. It is found that the submodelling-based global-local approach is the most efficient analysis technique for this case, capturing failure modes including delamination, core crushing and local surface indentation in the blade. The findings of this study can be used to develop accurate and computationally efficient tools for modelling impact-induced damage to a blade.

Keywords: Wind turbine blade, impact, finite element method, global-local method, progressive failure analysis

1. Introduction

Wind energy is one of the most prominent and sustainable renewable resources, both in onshore and offshore environments [1, 2]. In the past decade, the total global cumulative installed capacity of wind turbines has grown from 94 GW to 540 GW [3]. It is predicted that by 2030, wind energy will contribute to 29.6% of the entire EU's

*Corresponding author
Email addresses: amrit.s.verma@ntnu.no (Amrit Shankar Verma), nils.p.vedvik@ntnu.no (Nils Petter Vedvik), phih@dtu.dk (Philipp Ulrich Haselbach), zhen.gao@ntnu.no (Zhen Gao), zhiyu.jiang@uia.no (Zhiyu Jiang)

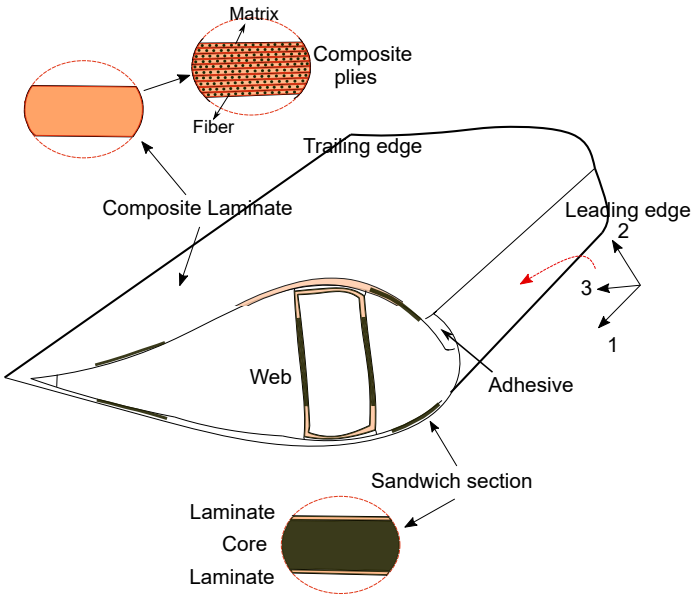

Figure 1: Material characteristics of a wind turbine blade

electricity demand [4] and will become the largest renewable energy source in Europe, exceeding the hydropower sector. The increased demand has led to an accelerated growth in the rated capacity of turbines, including rapid upscaling of the size of wind turbine blades. For example, the recently announced Heliade X-12 MW class of offshore turbines from General Electric (GE) will have a rotor diameter of more than 220 m with a blade length exceeding 100 m [5]. The upscaling of the blade length increases the energy output per unit of rotor swept area and is an economical choice, from a profitability perspective, of the wind industry. However, as the size increases, the loads on the blade also increase. This presents significant challenges and concerns regarding its life cycle, including the design, manufacturing, and installation phases.

A wind turbine blade design is a compromise between aerodynamic efficiency and structural strength requirements [6, 7]. This necessitates the application of composite laminates and sandwich sections (Fig. 1) in the blade owing to these materials' high merit index [8], thus imparting it with a high strength-to-weight ratio. Composite laminates encompass several composite plies, with each ply consisting of continuous fibres embedded in synthetic polymeric resins, and exhibit excellent in-plane structural performance in the fibre direction [9]. Similarly, a sandwich section is also a tailored arrangement of plies, though they are separated by a low-density thick core material (Fig. 1) and are provided in suitable sections of a blade to increase its bending stiffness and buckling resistance [8]. This tailored application and stacking of composite and sandwich sections in a blade satisfies its design strength requirements, taking into consideration the combination of aerodynamic, inertial, gyroscopic, and gravitational loads experienced during its service life [10].

Nonetheless, in addition to these operational loads, wind turbine blades are also exposed to numerous impact risks and loads arising from transverse impact forces applied by foreign objects [11]. These involve events ranging from frequently reported bird and hail collision strikes during operation to impacts with surrounding structures during transportation and installation [9]. One of the main concerns and restraints is the poor properties of the composite laminates and sandwich sections in the fibre off-axis and through-the-thickness directions [12]. These

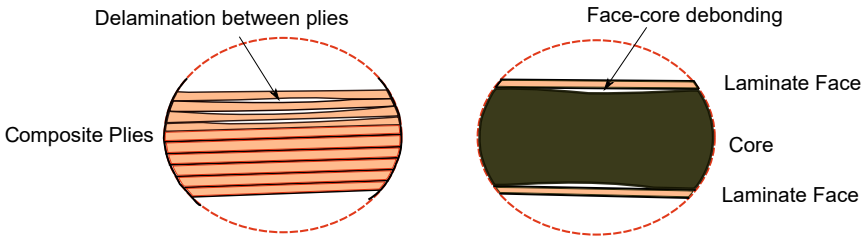

Figure 2: Delamination and face-core debonding

poor properties makes the blades highly vulnerable to transverse impact loads [11]. The shock waves arising due to such impact in a composite, unlike in metallic structures, cause many interacting and complex damage modes, which cannot always be visually inspected but can still grow under the action of normal operational loads [13]. Typical damage modes in a sandwich composite due to impact include the superposition of different intralaminar modes, e.g., matrix cracking and fibre failure, in the ply and core crushing as well as interlaminar damage modes such as delamination of the plies and face-core debonding [8]. Among all these damage modes, delamination (Fig. 2), where a composite laminate exhibits poor or no bonding between adjacent plies [14], is considered as one of the most critical failure modes. For example, in [14], it was found that delamination that developed closer to the laminate surface at the suction side of the blade could induce local sublaminate buckling, causing significant local strength and stiffness reductions. This could even lead to structural collapse of the blade because of high compressive loads that developed in these regions during its service life, with these delamination cracks susceptible to growth. Therefore, owing to the limitations of these materials in resisting impact loads and the associated high consequences, wind turbine blade design standards recognize impact loads as one of the major elements to be considered while designing wind turbine blades.

The design guidelines from DNV-GL [15] suggest that any impact load exerted on a blade should induce visible damages if it is critical for the strength of the blade. Otherwise, it recommends that the blade must be designed for maximum impact loads expected to occur during the service life. The guideline also gives special consideration to impact damages occurring in the blade during temporary phases like packaging, transportation and assembly procedures. Current industrial practice, due to lack of tools for estimating impact loads for different impact scenarios, utilizes high safety factors in the design calculations [8]. This approach is conservative and imposes a major disadvantage, requiring the local thickness at a section of the blade to be increased, with design strains kept low [16]. Better prediction methods and measurement systems that can reduce the high safety factors as well as the blade mass significantly are therefore required.

With the above in view, more advanced design techniques such as that based on damage tolerance conception [17, 18] are becoming more prevalent for designing wind turbine blades. Under this design approach, despite consideration of the high safety factors, a wind turbine blade is designed with pre-existing damage arising due to impact or manufacturing defects. It is then verified that the residual strength of the blade due to these defects is adequate and that a blade with pre-existing damage still meets the design strength requirements and will last through its design lifetime. However, to employ this design approach, estimation of the impact loads and nature and the extent of damage to a blade under different impact scenarios is required.

There are several approaches to tackling this problem, including experimental, analytical and numerical procedures. The experimental methods are costly, time consuming and not a feasible option, particularly in the design stage, where large combinations of scenarios and loading conditions exist [8]. Analytical approaches are often limited in their applications to complex structures and impact loads because they are usually only valid for simplified structures and ideal load assumptions. In comparison to these, numerical finite element methods (FEMs) and techniques provide more convenient, efficient and practical solutions to complex problems and is thus the focus of the paper. In this article, three different numerical modelling techniques, i.e., (1) pure shell, (2) shell-to-solid coupling, and (3) submodelling methods, for the impact investigation of a wind turbine blade are compared for a case where an impactor hits the leading edge. The remainder of the paper is as follows. Section 2 presents the problem statement, including a brief literature review on different techniques used in the study. Section 3 explains the analysis procedure. The materials and modelling methods are then introduced in sections 4 and 5. Section 6 presents the results and compares different modelling techniques. Finally, section 7 concludes the paper.

2. Problem statement and literature review

The impact modelling of a wind turbine blade or any composite structure in general can be categorised at two levels of structural detailing: an impact investigation at a representative coupon scale and an investigation of a full-scale composite structure (Fig. 3). The coupon scale refers to accurately defined standardized testing and modelling techniques established for laminates with simplified boundary conditions (e.g., ASTM-D7136 [19], Boeing BSS-7260 [20]). The full-scale composite structure, on the other hand, refers to a realistic structure, e.g., a wind turbine blade. These structures generally have complex boundary conditions with varying layup at different sections and have large inertia and flexibility associated with them. As a result, compared to the coupon representation, these structures store more energy elastically during impact, with less energy being dissipated as damage. Similarly, a wind turbine blade spans several metres from root to tip and has internal structural components consisting of caps and webs, which provide large flexibility during an impact (Fig. 3). It was found in [11] that 7-20% of the overall impact energy was absorbed as damage when a wind turbine blade collided with a tower during an offshore installation. Most of the energy, owing to high flexibility, dissipates as rigid body motion and rotation of the blade post-impact. Similar studies in the aerospace sector over the years [16, 21] also suggest that the results at the coupon scale are a poor indicator of the performance of a realistic structure under impact. Therefore, to simulate the impact response accurately, it is essential to consider the inertia, flexibility and complete elastic response of a composite structure. Numerical models are thus required to investigate the impact response in realistic structures at full scale.

In the literature [22, 23, 24, 25], most of the impact modelling techniques at the coupon scale are based on pure solid elements involving the discretisation of plies throughout the coupon length, with brick elements and their interfaces defined by cohesive formulations. However, this requires a adequate number of elements through-the-thickness (at least one element for each ply) [26]. This high level of discretisation makes the analysis computationally expensive. Lopes et al. [27] investigated the low-velocity impact of a falling object on a 24-ply flat rectangular laminate coupon with dimensions measuring 150 mm X 100 mm; the overall analysis time required more than 4 days on a cluster of 32 CPU workstations. This computational expense is not practical and affordable for wind turbine

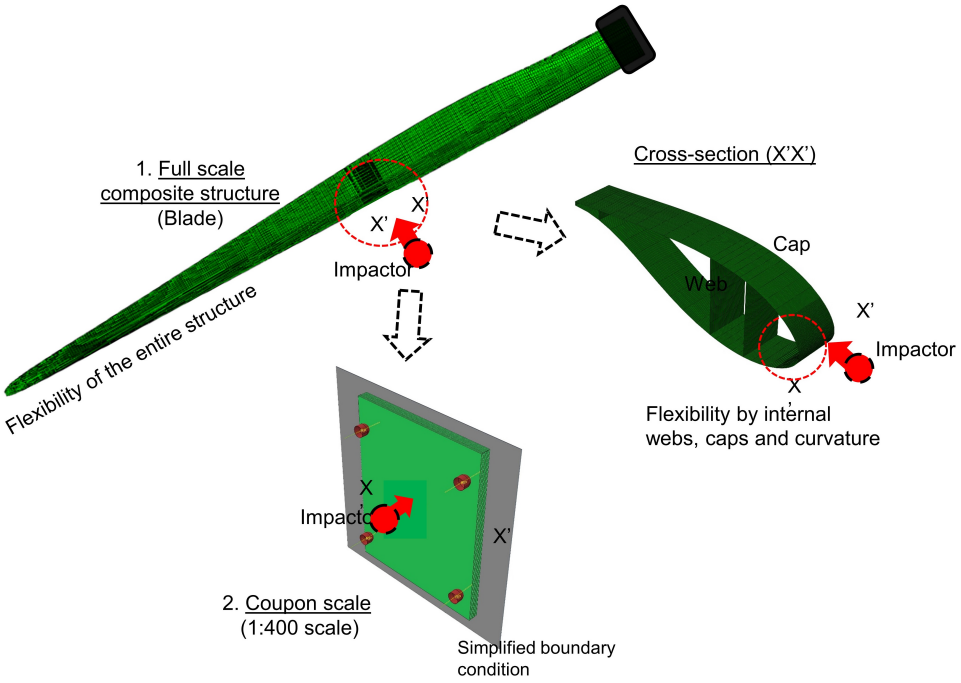

Figure 3: Different scale of impact investigation on a composite structure

blades, as they have large dimensions of over several metres with complex shapes and large contact areas with many plies, interfaces and thus many degrees of freedom. Hence, similar modelling methods in which an entire structure is discretised with solid elements is not an attractive option, especially for industrial use. Alternatively, there are other modelling techniques available that can be utilised. These primarily include pure-shell-element-based and multiscale-modelling-based global-local approaches. The present study compares the (1) pure shell, (2) shell-to-solid coupling, and (3) submodelling-based finite element modelling techniques for a case where an impactor hits the leading edge of a blade. A brief description of these techniques and their application in the published literature is given below.

The (1) *pure-shell-element*-based approach, owing to modelling and computational advantages, is one of the most simplified techniques for the impact modelling of a composite structure. Here, the structure is discretised by defining the geometry based on a reference shell surface (Fig. 4). The different plies through the thickness of the laminate are defined as a section property with integration points and specific material orientations. Since, the transverse shear stiffness of a composite is an important parameter to consider for its modelling, the shell elements, based on first-order transverse shear flexible theory, are employed [28, 29]. Although the theory assumes that the transverse shear strain through the thickness is constant, it is still possible to estimate interlaminar shear stresses through the thickness based on shear correction factors. This is employed for several thick shell elements (e.g., S4R elements) in Abaqus [30], where these stresses are derived as a post-processing output variable. Nachatne et al. [31] investigated a horizontal-axis tidal turbine under impact loads, where the GRP panels were discretised using thick S4R shell elements. The 2D Hashin failure initiation criterion [32, 33] was utilized to model intralaminar damage while considering the panel flexibility. Verma et al. [11] and Nanami et al. [34] also applied this approach

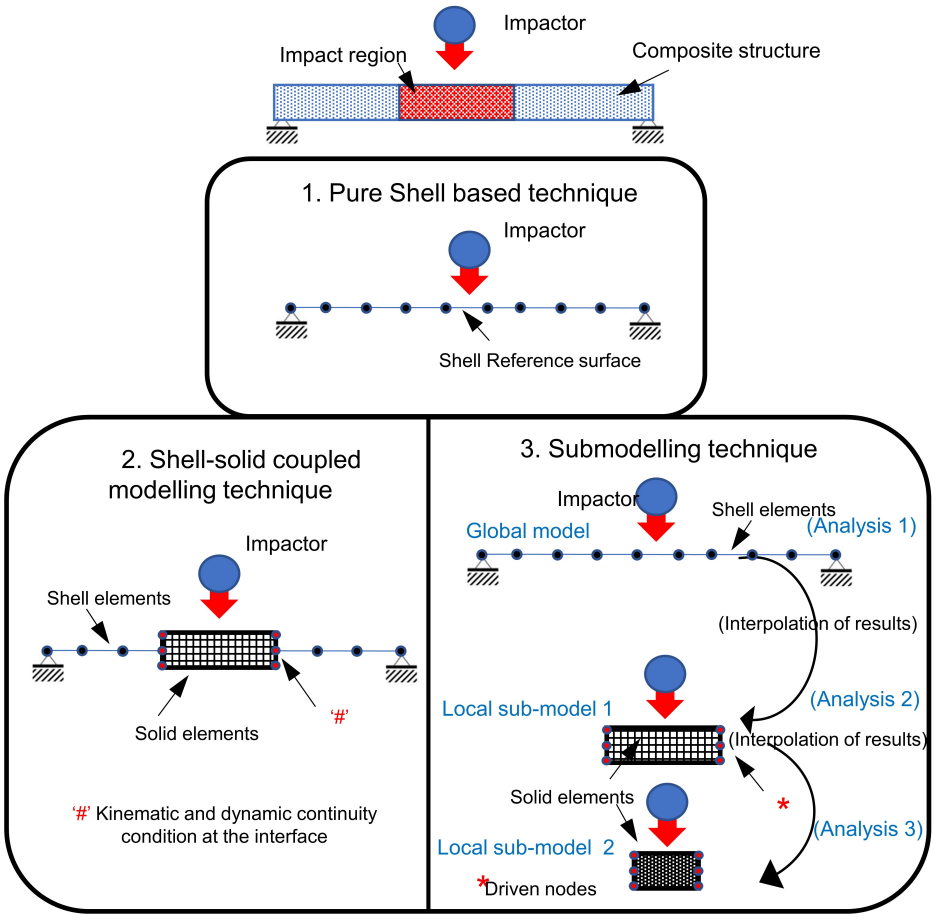

Figure 4: Fundamental principle behind different modelling techniques

to investigate scenarios where the leading edge of a wind turbine blade collides with a tower and is hit by a bird, respectively. The major disadvantage of this method is the inability of these elements to progressively model the separation of adjacent plies i.e. delamination occurring in a composite laminate [35]. Furthermore, this method cannot efficiently capture surface gouging effects [36] on the impact surface, as the elements of the model are removed only if all the plies (integration points) through the thickness satisfy the damage status.

On the other hand, there are also multiscale modelling approaches based on global-local methods that can be utilised for impact modelling of a composite structure. In these methods, refined meshing techniques with high-fidelity damage models are applied to regions of the structure (local domain), requiring detailed investigations. In contrast, the regions mainly contributing to the inertia (global domain) can be modelled with coarser meshes in finite element modelling. There are two widely utilized global-local methods, commonly known in Abaqus as the (2) shell-to-solid coupling method and (3) submodelling method.

The (2) *shell-to-solid coupling* or two-way transference tight coupling method [26, 37, 38] is a surface-based kinematic coupling constraint technique that enables the modelling of a structure using shell and solid elements within a given finite element model (Fig. 4). Here, the displacement and rotational degrees of freedom of the shell elements (global model) at the interface are coupled with displacement degrees of freedom of the solid elements (local model) [30]. This is achieved by creating internal sets of distributed coupling constraints between the reference nodes

on the shell edge and the coupling nodes at the solid surface. In this way, the forces and moments are distributed in a self-balancing manner from the reference node to the coupling nodes. The algorithm that Abaqus utilises to compute the internal coupling constraints with position tolerances, as well as its associated weighted averages, can be found in [30]. Haselbach et al. [14] used this feature to study the ultimate strength of a blade due to delamination developed on the suction side of a wind turbine blade. The local region at the suction side, measuring 1.4 m X 0.725 m, was modelled using C3D8R brick elements, with delaminated layers modelled using cohesive elements. The region was then coupled with the remaining blade, modelled using shell elements. Verma et al. [2] investigated the impact of a wind turbine blade root with the hub, with the T-bolt connection at the blade root being developed separately and modelled with solid elements. This was then coupled with other regions of the blade (modelled with shell elements) using the shell-to-solid coupling feature. Sun et al. [25] investigated the effects of the size and complexity of composite structures on impact behaviour, where the shell-to-solid coupling feature was validated via an experiment on a large-scale stiffened panel. The method showed good correlation with the experiment and demonstrated a high computational efficiency. The main advantage of this method is its intuitiveness, enabling the structure to have different fidelity levels in the same finite element model and thus requiring only one set of analysis. However, the major concern regarding this technique is the sensitivity of the elements at the transition zone between shell and solid meshes due to non-physical responses, which can lead to distortion [39]. This requires a careful modelling with a sensitivity-based selection of element sizes present in these regions to avoid any unrealistic stress concentrations. Another main disadvantage is that the local regions in structures, which are critical to get damaged, should be known a priori, as the high-fidelity local finite element models are embedded in the global model from the start of the analysis and exchange solutions together [26, 37, 38, 40].

The (3) *submodelling* or one-way transference loose coupling method enables the local part from a large structure to be extracted as a spatially separate model (Fig. 4); these local models are defined by a high-fidelity refined mesh and advanced material models and are separately analysed by transferring boundary conditions loosely from a global analysis. This technique is based on St. Venant's principle, which expresses that the result in the localized region (i.e. the submodel) is not affected by far field effects provided the end loads are statically similar. The link, which maintains this equivalency, is the displacement field that is obtained at the boundaries of a large structure from global analysis (Analysis-1) and is transferred to its local submodel's boundaries during submodel analysis (Analysis-2). The large structure is generally discretised with a coarser mesh (e.g., shell elements), on which the global analysis (Analysis-I) is performed. Shah et al. [41] developed an approach, where submodelling based technique was used to predict failure modes in a wind turbine blade at global scale and sensitive zones, under extreme loading conditions, were identified at local scale. A detailed list of sub-modelling strategies were presented, and results demonstrated good efficiency and were in close agreement with the experiments. Nie et al. [39] used this method to develop advanced models for investigating impact-induced damages in triaxially braided composites. Different levels of submodels were developed, and their displacement field equivalencies were compared with those of the global model. Furthermore, the numerical results and damages were verified via experiments, which demonstrated good correlation. The main advantage of the submodelling method is that different levels of detailed submodels for complex structural shapes can be studied independently. The method further helps to decide the size and location of a local submodel based on the results of a global analysis. One of the major issues

regarding this method is the accuracy in transferring the results from one analysis to another. This requires the submodel boundaries to be chosen far away from the locale where substantial variations of the responses occur in the global structure. Thus, displacement field equivalency at the global and submodel boundaries is one of the most important checks to confirm that the boundary conditions from the global analysis are correctly mapped onto the boundaries of the local submodel. Furthermore, the method allows only one-way information exchange between different models (global to local). Note that a two-way transference procedure was proposed by [37, 38], where information can be exchanged both ways.

3. Numerical analysis procedure

The discussions regarding the (1) pure shell, (2) shell-to-solid coupling, and (3) submodelling techniques suggest varying levels of accuracy for impact investigation, requiring different computational expenses, and therefore must be investigated. In this article, an attempt is made to compare these techniques to investigate a case where an impactor hits the leading edge of a wind turbine blade. This scenario corresponds to the case during offshore blade installation, where the leading edge is explicitly prone to impact/contact risks with surrounding structures and therefore is the main interest of the study [11]. Note that there are three facets for the impact investigation [42] of any composite structure in general: *impact response study* (considering the force, deflection and energy absorption), *impact resistance study* (considering the damages developed), and *damage tolerance study* (considering the residual strength post-impact). However, in this paper, the focus of the comparison of different modelling techniques for the impact investigation of a wind turbine blade is placed on the first two facets, i.e., impact response and impact resistance, along with the computational time required for each technique.

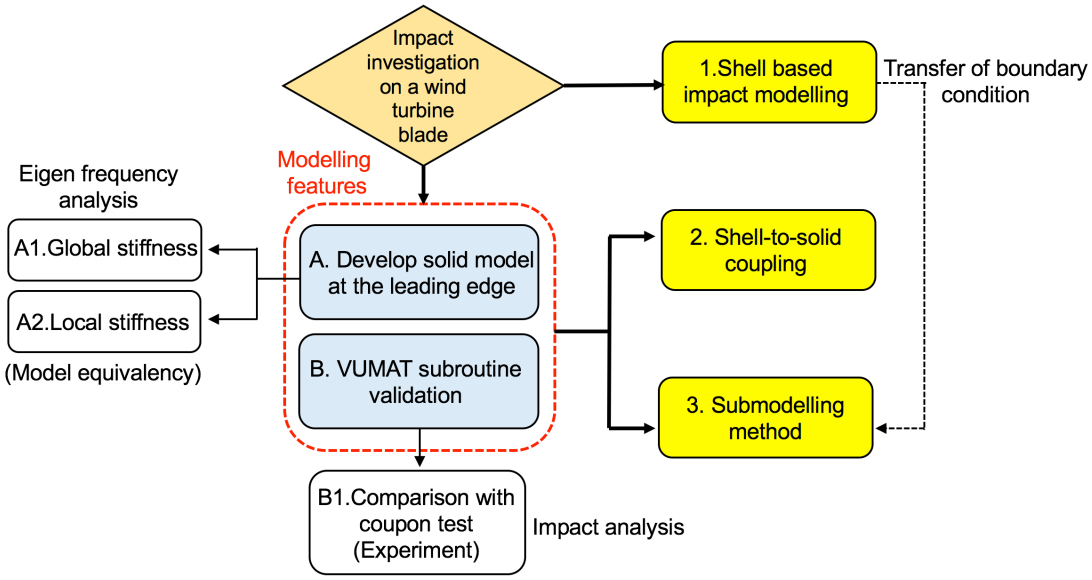

Figure 5: Numerical analysis procedure considered in the paper

Fig. 5 presents the analysis procedure considered in this work for comparing different modelling techniques for the impact investigation of a wind turbine blade. We utilise the DTU 10 MW reference wind turbine blade

as the base model, which is 86.4 m long and has its internal and external geometry completely discretised using shell elements. As a result, the (1) shell-element-based impact modelling technique is relatively straightforward. However, for the (2) shell-to-solid coupling and (3) submodelling methods, there are a few sets of modelling features that need to be developed as a prerequisite, which are discussed below (labelled as 'A' and 'B'; see the red dotted box in Fig. 5).

A. The first modelling feature is the development of a high-fidelity local solid part at the leading edge of the DTU 10 MW blade, with individual layers of plies and a core discretised using brick elements, at the region of impact. This local part will be utilized as the 'solid' finite element model for the leading edge while analysing the (2) shell-to-solid coupling and (3) submodelling techniques. Furthermore, the global (A1) and local (A2) stiffness characteristics of the modified blade are compared with those of the original DTU blade to validate the 'model equivalency'. In this article, the modelling technique for the development of the local solid part at the leading edge as well as the results confirming the model equivalency are also presented.

B. The next feature is the implementation of the Hashin 3D-failure initiation criterion for progressive damage modelling of the intralaminar failure modes in the composite laminates for the (2) shell-to-solid coupling and (3) submodelling techniques. For shell elements, the 2D Hashin criterion is already a built-in feature in Abaqus. However, for solid elements, a user-defined VUMAT subroutine is formulated in Fortran and is implemented in Abaqus. In this article, the validation of the subroutine accuracy via an experiment involving a coupon impact test taken from the published literature (B1) is also presented. Once these prerequisite parameters (A, B) are established and the results for A1, A2, and B1 (Fig. 5) are validated, impact investigations of a wind turbine blade based on these different modelling techniques are performed. The next section presents the modelling method for each step mentioned in the analysis procedure, each of which is presented according to the order in which it is discussed.

4. Modelling method

For the numerical study, we utilised the DTU 10 MW reference blade [43] as the basis for comparing different techniques in an impact investigation. The blade, described in [43], is made from glass fibre reinforced plastic (GFRP) laminates, with balsa as the sandwich core material. Its structural design is build upon a typical approach, with an internal load-carrying structure consisting of two caps and two shear webs. Furthermore, for the purpose of defining the material layup, the blade is partitioned radially into 100 cross-sections (numbered from SEC-1 to SEC-100), and each section is further separated into 11 distinct regions along its circumference. The layup is characterised by smearing properties and has a stacking plan in terms of multidirectional plies. The entire blade is discretised originally with shell elements having reference shell surface along the outer surface of the blade (node offset = -0.5), which corresponds to its aerodynamic profile. This was done to account for the continuously changing thickness of the layup [14]. Also, the blade has no explicit adhesive connection defined in any region, except for some regions at the trailing edge. Note that the leading edge of the blade, which is the region of interest in this study, is designed as a sandwich section and is fused with balsa.

A. Local solid part at the leading edge

The region of the leading edge (highlighted in red in Fig. 6) chosen for the local solid part, where the impact is considered, corresponds to section no. 42, 43 and 44 of the DTU 10 MW blade and represents the region of the DTU 10 MW blade spanning between 38.2 m to 40.8 m relative to the radial position of the blade root.

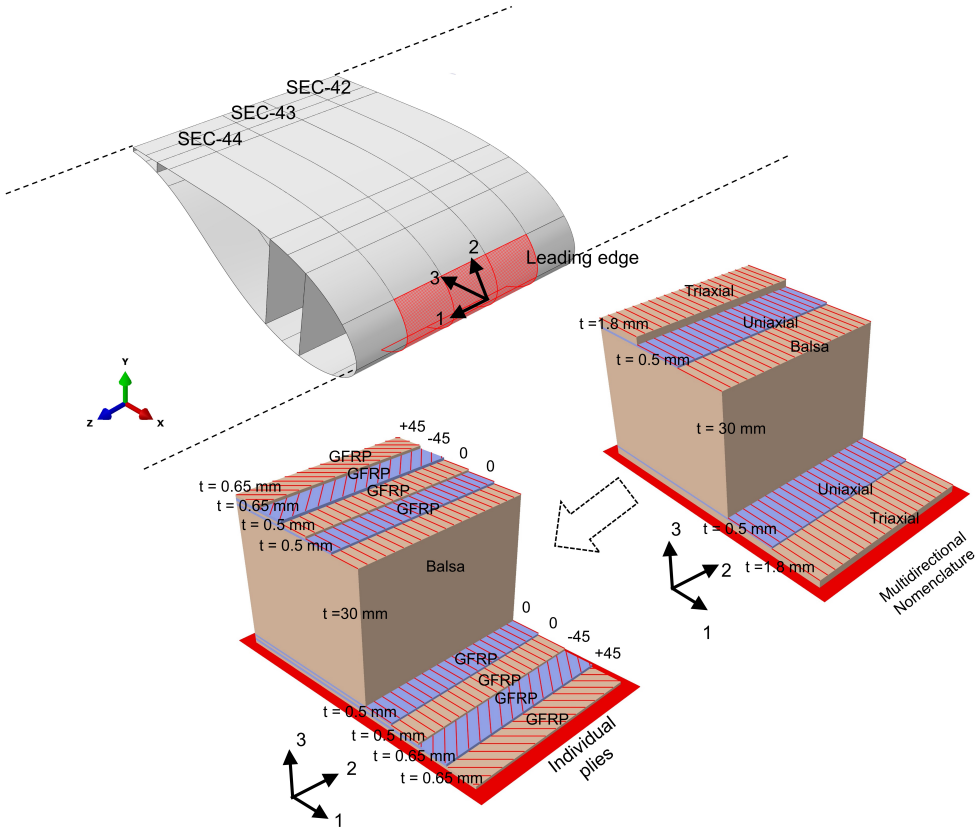

Figure 6: Region of the leading edge considered for local solid part with parent and modified layup

To develop the local solid part, the first crucial piece of information is the composite layup, with the stacking sequence of the laminate defined in terms of the individual plies. This information will determine the thickness, number of layers, cohesive interfaces and material orientation of brick elements in the local solid part. The layup in this region for the DTU 10 MW blade is, however, initially defined by multidirectional plies, and the stacking sequence has the form $[\text{Triaxial/Uniaxial/Balsa}]_s$ (Fig. 6). According to [23], a triaxial ply can be approximated to the equivalent properties of individual plies oriented in [+45/-45/0] with 35%, 35% and 30% contributions, respectively, whereas uniaxial plies can be approximated to the equivalent properties of individual plies oriented in [0/90] layers with 95% and 5% contributions, respectively. These multidirectional plies correspond to the smearing properties and cannot be explicitly utilised for progressive damage modelling, as they would be unable to predict the impact response of individual plies subjected to impact. Fig. 6 presents the layup derived at the chosen region of the leading edge (SEC-41, SEC-42, SEC-43) in the form of the individual-ply-based stacking sequence: $[+45/\text{-}45/0_2/\text{Balsa}]_s$. This layup was obtained via an iterative procedure, which transforms a multidirectional-based stacking sequence back into its individual plies while keeping the parent parameters, e.g., mass of the blade, COG

of the blade and thickness of the section, consistent. The details and validation of this iterative procedure have already been presented in a previous work [11] and can be referred to for more information.

Based on the derived stacking sequence presented in Fig. 6, a local solid part at the leading edge with dimensions of 2.6 m X 0.96 m and a thickness of 34.6 mm was developed by using the mesh offset option in Abaqus (Fig. 7). Several layers of solid C3D8R brick elements corresponding to GFRP top and bottom laminate face sheets and the balsa core were generated on the parent shell surface. Furthermore, the local solid part was divided into two separate regions – a central inner mesh (I) and an outer transition mesh (II), which were tied together using tie constraints (Fig. 7). The element size in the transition region was kept relatively coarse (with a 2:1 ratio) compared to the element size in the inner mesh region. This was done to account for computational efficiency as well as to fulfil the requirement of a transition region for the shell-to-solid coupling technique [14]. The interfaces among plies with different fibre orientations as well as the interface between the laminate face and the core were characterized by cohesive-surface-based interactions. This was implemented to account for delamination between plies or face-core debonding developing due to impact. Finally, the complete meshing procedure was automated using a python-based script that controls the extent of these regions (I, II) of the local solid part and their element sizes.

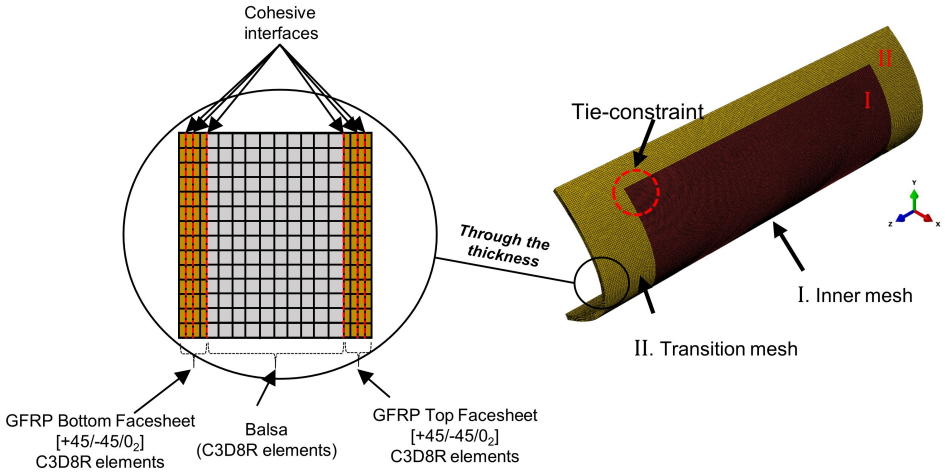

Figure 7: Local solid part with individual layers

A1. Global stiffness of parent and modified blade

The modelling equivalency between the original DTU blade with shell elements and the modified blade with an embedded high-fidelity local part was validated to confirm that the global stiffness of the modified blade had the same characteristics and was not influenced by altering the parent blade. For this, an eigenfrequency analysis was performed on the modified blade, with the local solid part connected to its remaining shell region by the shell-to-solid coupling technique (Fig. 8). The blade root was fixed relative to all degrees of freedom, and a linear perturbation step based on the Lanczos solver was performed. The analysis was run on an HPC machine with one node and 20 CPUs and required 40 hours to extract the natural frequencies of the modified blade in the flapwise and edgewise modes.

A2. Local stiffness of leading edge section with shell and solid elements

The local stiffness of the leading edge section discretised using brick elements (local solid part) was compared with the corresponding leading edge section of the parent DTU blade discretised using shell elements. This comparison

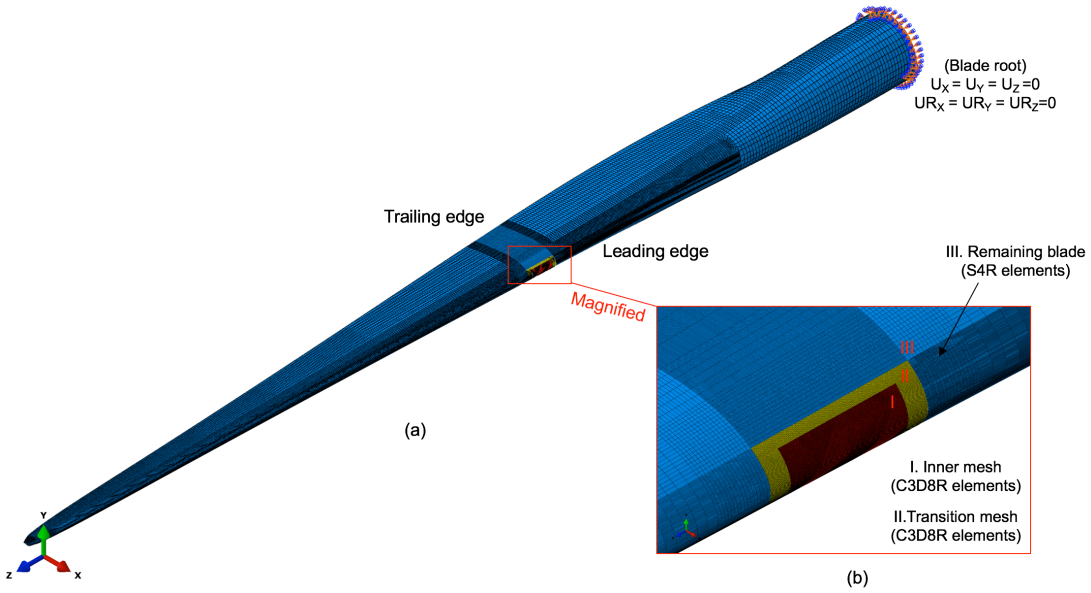

Figure 8: (a) Eigen frequency analysis of the modified blade with embedded local solid part (b) Enlarged view

was conducted to validate the model equivalency between the shell- and solid-element-based sections so that the impact investigation results for the leading edge based on different elements could be compared. The eigenfrequency analysis was performed (Fig. 9) on the leading edge shell section and the developed local solid part. Both models had pinned joints, and a linear perturbation step with the Lanczos solver scheme was employed to extract the natural frequencies.

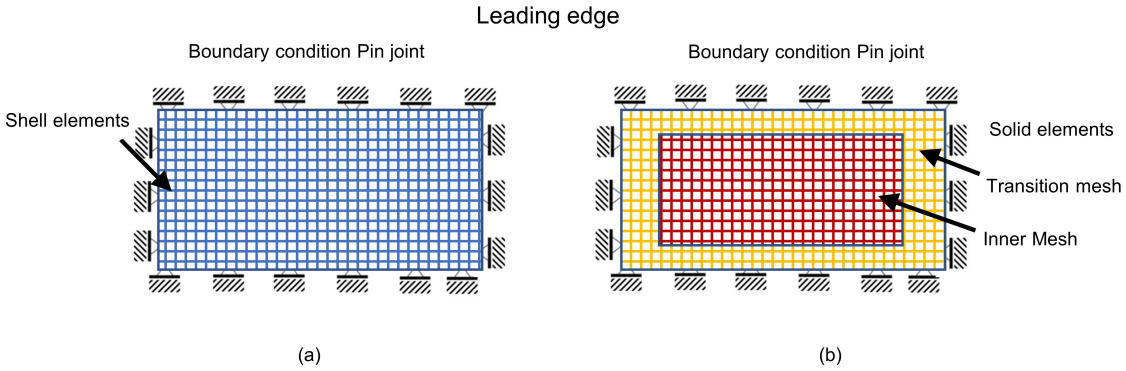

Figure 9: Eigen frequency analysis on the leading edge (a) Shell elements (b) Solid elements

B. VUMAT subroutine validation for progressive damage modelling of composite laminates

The Hashin failure criterion [32] was used in this study to perform a progressive damage modelling of the intralayer failure modes in a composite laminate at the ply level. A VUMAT subroutine based on this criterion was

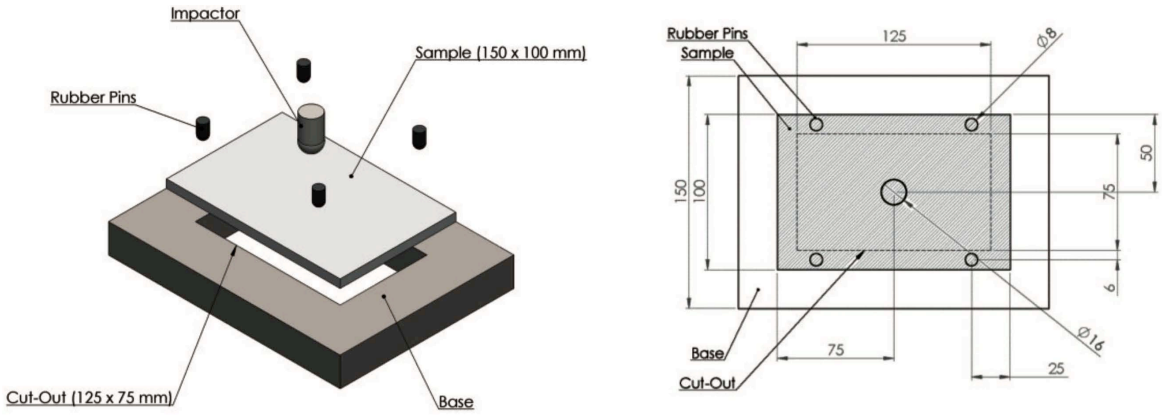

Figure 10: Experimental set up as reported in [24]

formulated in Fortran and implemented in Abaqus. Here, the details of the modelling technique used to validate this subroutine, with an experiment from the published literature, are presented. Perillo et al. [24] investigated the low-velocity impact response on stitch-bonded GFRP composite plates comprising thick laminates. The laminates were produced using the vacuum infusion process, which is commonly utilised in the wind turbine blade industry. A series of impact tests corresponding to different impact energy levels as per the ASTM [19] guidelines was performed. The experimental setup reported in [24] is shown in Fig. 10.

Fig. 11 presents the numerical model of the test we created in Abaqus/Explicit, where the specimen with the stacking sequence $[0/90/90/0]_s$ and dimensions of 150 mm X 100 mm with a total thickness of 6.8 mm was discretised using C3D8R brick elements. The interfaces among plies with different fibre orientations were defined

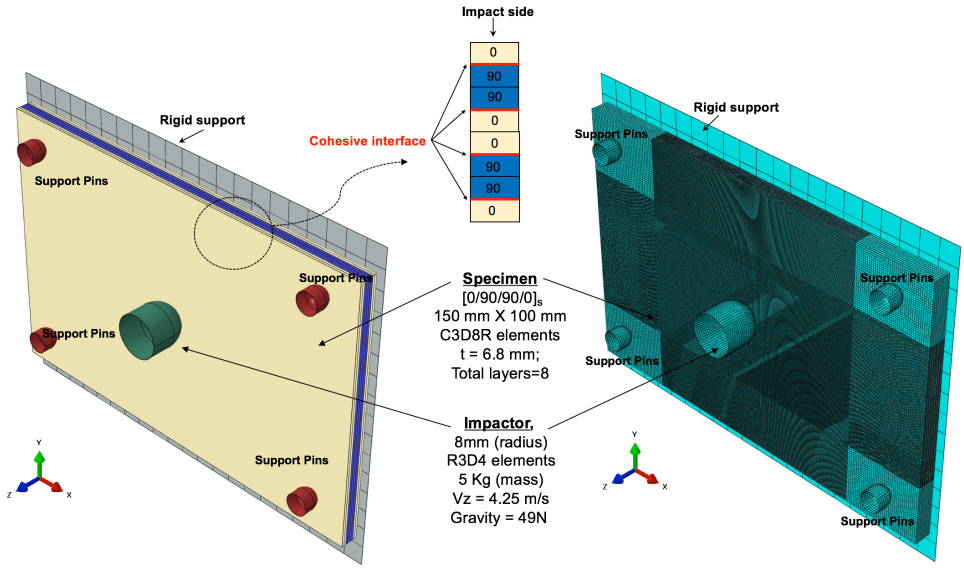

Figure 11: Numerical modelling of experimental set up based on [24]

with cohesive-surface-based interaction behaviour, which enabled modelling the interlaminar failure mode, i.e., delamination. The damage initiation was defined by quadratic stress failure criterion along with BK (Benzeggagh-Kenane) energy-based damage evolution law for mixed opening mode and $\eta = 1.45$ was considered. The material

properties utilised for the intralaminar and interlaminar composite plies are reported in Table 1. Furthermore, for the impact investigation, the impactor was defined as a rigid body with a reference point assigned to it. The

Table 1: Material properties for GFRP laminate (HiPer-Tex R-Glass fiber with EPIKOTE MGS 135 resin) [24]

ρ	E_{11}	$E_{22} = E_{33}$	$\nu_{12} = \nu_{13}$	ν_{23}	$G_{12} = G_{13} = G_{23}$
1230 kg/m^3	44.87 GPa	12.13 GPa	0.3	0.5	3.38 GPa
X^T	X^C	$Y^T = Z^T$	$Y^C = Z^C$	$S^{12}=S^{13}=S^{23}$	G_{IC}
1006.3 MPa	487 MPa	45.95 MPa	131.90 MPa	49.51 MPa	9810 J/m^2
$G_{IIC} = G_{IIIC}$	t_n^o	$t_s^o = t_t^o$	η		
3710 J/m^2	45.95 MPa	49.51	1.45		

reference point was assigned an inertial mass of 5 kg and was given an initial impact velocity of 4.25 m/s (V_z), which corresponds to 45.5 J of impact energy. Furthermore, the specimen was supported on a flat rigid support, modelled as rigid body, which was constrained relative to all degrees of freedom. There were four supporting pins, also modelled as rigid body elements, which were utilised in the model to give a more accurate representation of the boundary condition on the specimen, as reported in the actual test [24]. The contact between the individual layers of plies in the specimen, impactor, support and pins was defined using a general contact scheme, with a penalty algorithm and a friction value equal to 0.3 being used. Finally, the model had approximately 240K C3D8R elements with an element size of 1 mm X 1 mm (two elements through the thickness for each ply) in the region of impact.

Impact modelling techniques for wind turbine blade

Three different modelling methods based on the (1) pure shell element, (2) shell-to-solid coupling, and (3) submodelling techniques were evaluated. For comparison, only the region of the blade corresponding to sections 42, 43 and 44 was considered in the finite element study owing to the size of the impactor, which is significantly smaller compared to the overall size of the blade (Fig. 12). Also, note that in this study, the impact is considered of rebounding nature rather than penetrating type and this corresponds to impact scenario during blade installation, which is mentioned earlier as the main motivation for the study. A sensitivity study was also carried out, and the region chosen was far away from the location of impact to ensure no influence on the local impact response.

The modelling methods utilised for the different techniques in the impact investigation are described here. Note that in this study, the Abaqus/Explicit solver is utilised, owing to the solver's efficiency in handling highly nonlinear problems involving complex interactions, large rotations and large deformations.

For (1) the pure shell-element-based approach (Fig. 12), the entire blade, including the region of impact at the leading edge, was discretised using 4-node thick shell (S4R) elements with reduced integration scheme. The region of impact had a refined mesh with an element size of 5 mm X 5 mm. The region of the blade far away from the impact was modelled with a coarser mesh for computational efficiency. To simulate a realistic contact between the impactor and the exterior surface of the blade during impact, the aerodynamic profile of the blade was considered as the reference surface for the shell element. The region of impact was characterized by a stacking sequence with a layup: $[+45/\text{-}45/0_2/\text{Balsa}]_s$. Each of the plies were defined with three integration points; thus, having in total

27 integration points through the thickness in the region of impact. The blade was defined as being fixed, with its edges constrained relative to all degrees of freedom. Furthermore, a rigid body impactor with a radius of 0.1 m and mass of 30 kg was discretised with 4-node, bilinear quadrilateral rigid (R3D4) elements and was associated with a reference point. The reference point was defined with an initial velocity in the X-direction (V_x) and was

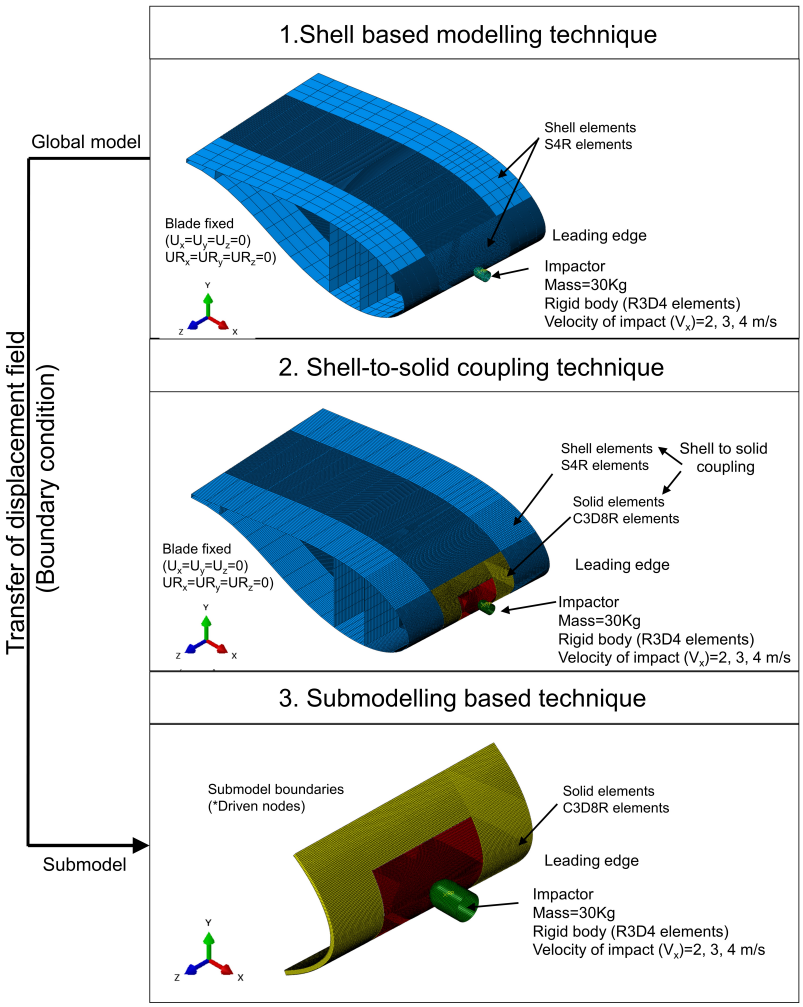

Figure 12: Impact modelling of blade based on different techniques

further constrained relative to other degrees of freedom (U_y=U_z=0; UR_x=UR_y=UR_z=0). The contact between the impactor and the leading edge was defined by a general contact scheme in Abaqus using a penalty algorithm with a friction coefficient value equal to 0.3. Three cases of impact velocities representing different impact energy levels (V_x =2 m/s, 3 m/s, 4 m/s; KE_{impact}= 60 J, 135 J, 240 J) were considered. Finally, an analysis was performed on a supercomputer with a cluster of 2 nodes. Note that the computational resources were kept the same for all the modelling techniques to allow comparing the amounts of time elapsed in the analysis.

For the (2) shell-to-solid coupling technique (Fig. 12), the high-fidelity local solid part consisting of an outer transition (II) and a central inner mesh (I) region, with individual layers discretised using brick elements, was utilised. This local solid part corresponds to the true thickness of the leading edge and was substituted in the

parent DTU blade in the region of impact. The transition region (II) of the local solid part was discretised using standard continuum hexahedral (C3D8R) solid elements having eight nodes and a size of 10 mm X 10 mm. This region was made flush with respect to the reference top surface of the adjacent shell region of the leading edge (III) by using the shell-to-solid coupling feature (Fig. 13). The inner mesh (I) was also discretised with C3D8R elements and had a relatively finer mesh of 5 mm X 5 mm. The region was connected to the transition region via a tie constraint, which enabled the two regions to act as one part despite having varying element sizes. The contact was defined between the impactor and all the plies of the local solid part along with cohesive surface based interaction defined at the interfaces of the differentially oriented plies and at the face-core interface. The hard contact pressure overclosure behaviour along with penalty algorithm and friction coefficient of 0.3 was used under general contact scheme in Abaqus/Explicit. The contact stiffness properties of the ply interfaces and face-core interfaces were assumed to be similar. Boundary conditions similar to those used in the (1) shell-based modelling method were employed, with the blade edges being fixed and the rigid impactor being given an initial velocity in the X-direction. Also, to maintain a stable aspect ratio for the brick elements, the plies at the top and bottom face sheets were discretised with single element in the thickness direction.

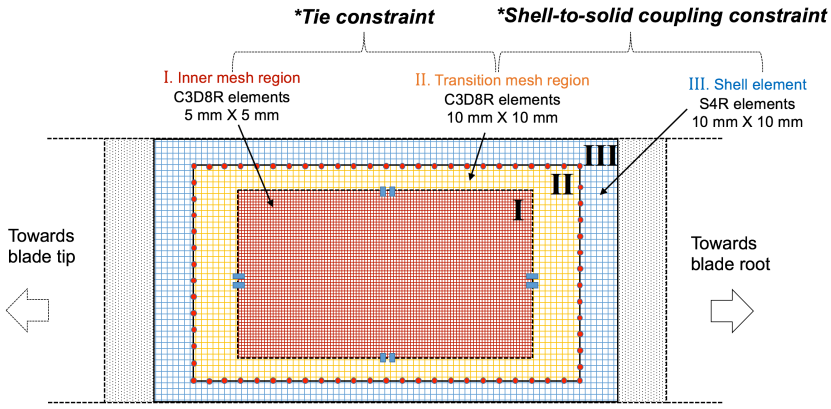

Figure 13: Illustration of shell-to-solid coupling technique utilised at the leading edge

For the (3) submodelling method, the local solid part consisting of an inner mesh region and a transition mesh region was used as the submodel, having precisely the same dimensions as those utilised for the (2) shell-to-solid coupling technique. Although the extent of the submodel region in general varies with the results based on global analysis, equivalent dimensions were considered for the submodel such that the computational time required in the analysis could be compared with that of other techniques considered in this study. Nevertheless, the boundary of the submodel was found far away from the locale where substantial variations of the responses occurred and thus was considered suitable. The submodelling analysis is based on a multi-step analysis, where the displacement boundary conditions are transferred from the global analysis to the submodel analysis. Thus, firstly a global analysis based on (1) shell-based impact modelling was performed. A significantly large amount of output frames were requested during the global analysis to extract the variation of the displacement field at the driving nodes of the global shell model. This prevents any potential aliasing effects due to the transfer of boundary conditions. The displacement field obtained was enforced as the submodel boundary condition in submodelling analysis on the driven nodes of the

submodel. The time step for both the analyses were considered same. The other modelling perspectives, such as the boundary conditions and initial velocity assigned to the impactor, the element size and the contact definitions, were kept equivalent to those of the (2) shell-to-solid-coupling-based impact modelling technique.

5. Implemented constitutive damage models

We utilised in this study damage models which are suitable for modelling impact induced failure modes in a sandwich composite. These involve combinations of intralaminar damage modes (matrix cracking and fiber failure in individual plies), interlaminar damage modes (delamination at ply interfaces, face-core debonding) and damage modes associated with core (shear failure, core crushing). Note that, we consider non-perforating type of impact loads.

5.1. Intralaminar damage model

The intralaminar failure modes that develop in a composite ply due to impact were modelled in the finite element analysis by utilising the Hashin failure criterion [32]. This criterion is one of the most widely utilised damage models for predicting failure in a composite laminate owing to its capability to distinguish between different failure modes at the ply level while considering the interaction between different stress components. This criterion is already a built-in feature in Abaqus for the progressive damage modelling of unidirectional fibre composite plies; however, the feature is reserved for elements with plane stress formulations, e.g., shell elements [30]. For damage modelling based on 3D-solid elements and to enable the application of failure criteria in the (2) shell-to-solid coupling and (3) submodelling methods, a user material VUMAT subroutine was formulated in Fortran and implemented in Abaqus. Note that the failure criteria for both shell and solid elements in this study are described by the Hashin criterion; however, the implementation in Abaqus differs for these elements. The Hashin failure criterion for elements based on plane stress formulations does not consider through-the-thickness transverse normal stresses and interlaminar shear stresses ($\sigma_{33} = \sigma_{13} = \sigma_{23} = 0$) in the equations presented below. The four distinct intralaminar failure modes, as described by the Hashin failure criterion, are as follows:

1. Fibre failure in tension ($\sigma_{11} \geq 0$):

$$F_{ft} = \left(\frac{\sigma_{11}}{X^T}\right)^2 + \kappa\left(\frac{\tau_{12}}{S^{12}}\right)^2 + \kappa\left(\frac{\tau_{13}}{S^{13}}\right)^2 \geq 1 \tag{1}$$

2. Fibre failure in compression ($\sigma_{11} < 0$):

$$F_{fc} = \left(\frac{\sigma_{11}}{X^C}\right)^2 \geq 1 \tag{2}$$

3. Matrix failure in tension ($\sigma_{22} + \sigma_{33} \geq 0$):

$$F_{mt} = \left(\frac{\sigma_{22} + \sigma_{33}}{Y^T}\right)^2 + \frac{1}{(S^{23})^2}(\sigma_{23}^2 - \sigma_{22}\sigma_{23}) + \left(\frac{\tau_{12}}{S^{12}}\right)^2 + \left(\frac{\tau_{13}}{S^{13}}\right)^2 \geq 1 \tag{3}$$

4. Matrix failure in compression ($\sigma_{22} + \sigma_{33} < 0$):

$$\begin{aligned} F_{mc} = &\left(\frac{\sigma_{22} + \sigma_{33}}{2S^{23}}\right)^2 + \left(\frac{\sigma_{22} + \sigma_{33}}{Y^C}\right)\left[\left(\frac{Y^C}{2S^{23}}\right)^2 - 1\right] \\ &+ \frac{1}{(S^{23})^2}(\sigma_{23}^2 - \sigma_{22}\sigma_{23}) + \left(\frac{\tau_{12}}{S^{12}}\right)^2 + \left(\frac{\tau_{13}}{S^{13}}\right)^2 \geq 1 \end{aligned} \tag{4}$$

where σ_{11}, σ_{22}, and σ_{33} are normal stresses; τ_{12}, τ_{13}, and τ_{23} are shear stresses; X^{T} and X^{C} are the tensile and compressive strengths of the ply in the principal fibre direction, respectively; Y^{T} and Y^{C} are the tensile and compressive strengths of the ply in the transverse fibre direction, respectively; S^{12}, S^{13} and S^{23} are the in-plane and interlaminar shear strengths; and κ is the shear stress factor contributing to failure of the fibre under tensile stress.

Modelling intralaminar damage modes in this study based on the above formulation was done via a progressive failure analysis. It was assumed that the linear elastic stress strain relations followed orthotropic damage elasticity, where the undamaged stiffness matrix in the finite element model was evaluated by the classical theory of elasticity [24]. The damages in the ply that developed due to impact were calculated at each integration point and at every time step of the simulation. In the case of an element satisfying the failure state in any distinct failure mode due to impact, the stiffness matrix of the finite element model was progressively degraded. In this case, the initial undamaged elastic constants were reduced linearly, along with the damage variables calculated for the fibre failure and the matrix tension estimated from the Hashin failure criterion presented above.

5.2. Interlaminar damage model

Interlaminar failure modes in a typical sandwich composite consist of delamination and debonding occurring in the laminate and at the face-core interfaces, respectively. They were modelled in (2) shell-to-solid coupling and (3) submodelling based analysis by defining the interface properties in the local solid part with cohesive zone method (CZM) based constitutive relations. A surface-based cohesive behaviour, along with the classical energy-based bi-linear traction separation law, was considered. A linear elastic traction-separation regime was considered, for which the initial normal and tangential stiffness components for the interfaces were derived from [14]. The damage initiation was defined by a quadratic nominal stress criterion, where the damage is initiated when the contact stress ratios given by the quadratic interaction function become 1. This is given by:

$$\left\{\frac{\langle t_n\rangle}{t_n^o}\right\}^2+\left\{\frac{t_s}{t_s^o}\right\}^2+\left\{\frac{t_t}{t_t^o}\right\}^2=1 \tag{5}$$

where $\langle . \rangle$ is the Macaulay bracket, which is considered in the above equation to avoid any damage that may develop due to the compressive state of stresses. t_n is the normal contact stress in pure normal mode; t_s and t_t are the shear contact stresses in the first and second shear directions, respectively; and t_n^o, t_s^o, and t_t^o are the normal and shear strength parameters. Once the damage initiation criteria are met, an energy-based damage evolution law, which considers linear softening in the cohesive stiffness response of the interface post-damage, is implemented. The BK fracture criterion, which accounts for the dependency of fracture energy on the mode mix, is considered and has the following form:

$$G_{IC}+(G_{IIC}-G_{IC})\Big(\frac{G_{shear}}{G_T}\Big)^{\eta}=G_{TC} \tag{6}$$

where $G_{shear}=G_{II}+G_{III}$ and $G_T=G_I+G_{II}+G_{III}$. G_{IC}, G_{IIC}, and G_{IIIC} are the critical energy release rates for a crack in the mode I, mode II and mode III opening modes. G_{shear} is the energy released through the shear modes, and G_T is the total energy released. η is the cohesive property factor, which is assumed to equal 1.45. The material parameters utilised in this study are given in Table 2 and Table 3.

Table 2: Material properties of unidirectional GFRP laminate (E-Glass fiber with epoxy based resin), where ρ is the density, E is the Young's modulus, ν is the Poisson's ratio, $\boldsymbol{G}$ is the shear modulus, G_{ij} is the Fracture energy, X, Y and S are longitudinal, transverse and shear strength parameter respectively; 1,2 and 3 is the blade's longitudinal, transverse direction and out of plane direction [14, 43]

ρ	E_{11}	E_{22}	E_{33}	ν_{12}	ν_{13}	ν_{23}
1900 kg/m^3	41.63 GPa	14.93 GPa	13.43 GPa	0.2410	0.2675	0.33
$\boldsymbol{G_{12}}$	$\boldsymbol{G_{13}}$	$\boldsymbol{G_{23}}$	G_{ft}	G_{fc}	G_{mt}	G_{mc}
5.047 GPa	5.047 GPa	5.047 GPa	120000 J/m^2	67000 J/m^2	920 J/m^2	920 J/m^2
X_T	X^C	Y^T	Y^C	S^{12} =S^{13}=S^{23}		
903.60 MPa	660 MPa	42 MPa	42 MPa	58.65 MPa		

Table 3: Interface cohesive properties implemented in the study, where K is the interface stiffness, t is the maximum traction, G_C is the critical energy release rate, η is the cohesive factor for mixed mode [14]

K_{nn}	K_{ss}	K_{tt}	t_s^o	t_n^o
3e14 N/m^3	1.15e14 N/m^3	1.15e14 N/m^3	53 MPa	58.65 MPa
t_t^o	G_{IC}	G_{IIC}	G_{IIIC}	η
58.65 MPa	200 J/m^2	1000 J/m^2	1000 J/m^2	1.45

Table 4: Material properties of Balsa taken from [43, 44, 45, 46, 47]

ρ	E_{11}	E_{22}	E_{33}	ν_{12}	ν_{13}	ν_{23}
110 kg/m^3	0.050 GPa	0.050 GPa	2.73 GPa	0.5	0.013	0.013
G_{12}	G_{13}	G_{23}	S_L	S_T		
0.0167 GPa	0.150 GPa	0.150 GPa	2 MPa	2 MPa		

5.3. Constitutive material model for balsa core

An ideal constitutive material model suitable for analysing the impact response of a complex cellular material like balsa is a topic of ongoing research and is continuously evolving [28, 44]. This model requires consideration of factors such as anisotropicity, compressibility, softening, densification and strain rate dependency. Most importantly, during impact, the out-of-plane shear stress (τ_{13}, τ_{23}) distribution of the core significantly influences the response of the sandwich structure and is thus must be considered in the analysis. Plane stress elements do not consider the variation of transverse shear stresses in their formulations; however, for the thick shell elements in Abaqus, these out-of-plane shear stresses can be estimated at section integration points using shear correction factors and are obtained as post-processing output variables (TSH13, TSHR23). These can then be compared with the critical shear stress in the core to predict core shear failure. Haselbach et al. [48] utilised this approach while investigating the shear failure in a core due to buckling in addition to utilising plane stress formulations. The present paper considers this formulation for balsa for impact modelling based on (1) pure shell elements. On the other hand, for three-dimensional solid elements, Weijmar et al. [45] and Deshpande et al. [49] considered a crushable foam plasticity model to analyse the impact responses in the core. The densification zone of the balsa post-plasticity was

incorporated, and balsa was considered as transversely isotropic, which is a sound and practical assumption [28]. In addition, the results were compared with those of the experiments, demonstrating a good correlation. The present paper therefore utilises crushable foam plasticity with an isotropic hardening model [30] to analyse failure in the balsa based on the (2) shell-to-solid coupling and (3) submodelling techniques. The formulation of this model is based on an elliptical yield surface [30] centred at the origin in the meridional stress ($\sigma_p - \sigma_q$) plane, which evolves symmetrically (flow rule) about its centre as:

$$\sigma_q^2 + \nu^2 \sigma_p^2 = Z^2 \tag{7}$$

where σ_p and σ_q are the pressure and von Mises stresses, respectively, and ν and Z are the shape factor of the yield surface and the size of the ellipse in the σ_q-axis (i.e., ordinate axis) direction, respectively [30]. These factors are given by:

$$\nu = \frac{3k}{\sqrt{9 - k^2}} \quad \text{and} \quad Z = \sigma_c \sqrt{1 + \left(\frac{\nu}{3}\right)^2} \tag{8}$$

Here, k is defined as the yield stress ratio, i.e., the ratio between the initial yield stress of the material under uniaxial compression and that under the corresponding hydrostatic compression, and σ_c is the absolute value of the yield stress under uniaxial compression. In this study, the parameter k was taken as 1. Furthermore, the data points corresponding to true stress-logarithmic strain for balsa and the corresponding material strength parameter were derived from [44, 46, 47] and are reported in Table 4.

6. Results and discussion

The results confirming the modelling equivalency between the original and modified blade (A1, A2), and the validation for the implemented VUMAT subroutine based on Hashin failure criterion (B1) are presented first. Then the results for impact investigation on a wind turbine blade based on (1) pure shell (b) shell-to-solid coupling, and (3) submodelling method are presented and compared.

A1. Comparison of global stiffness between parent and modified blade

To illustrate the modelling equivalency between the modified blade (with a high-fidelity local solid part at its leading edge) and the original DTU blade (completely based on shell elements), their eigenfrequencies and corresponding eigenmodes are compared. These metrics present a significantly strong match between both blades, as shown in Fig. 14, where the eigenfrequencies and fringe plots for their corresponding first and second flapwise and edgewise modes are presented. Fig. 15 further summarizes the eigenfrequencies of the blades in eight major eigen modes, indicating a sound coherence between the global stiffness characteristics of the parent DTU blade and those of the modified blade.

A2. Comparison of the local stiffness between the leading edge section modelled with shell elements and that modelled with solid elements

The high-fidelity local solid part developed for the leading edge in the region of impact corresponds to only 3.2% of the entire blade length and corresponds to less than 1% of the total blade mass. The global eigenfrequency analysis presented above is not enough to validate the local stiffness and model equivalence for the leading edge

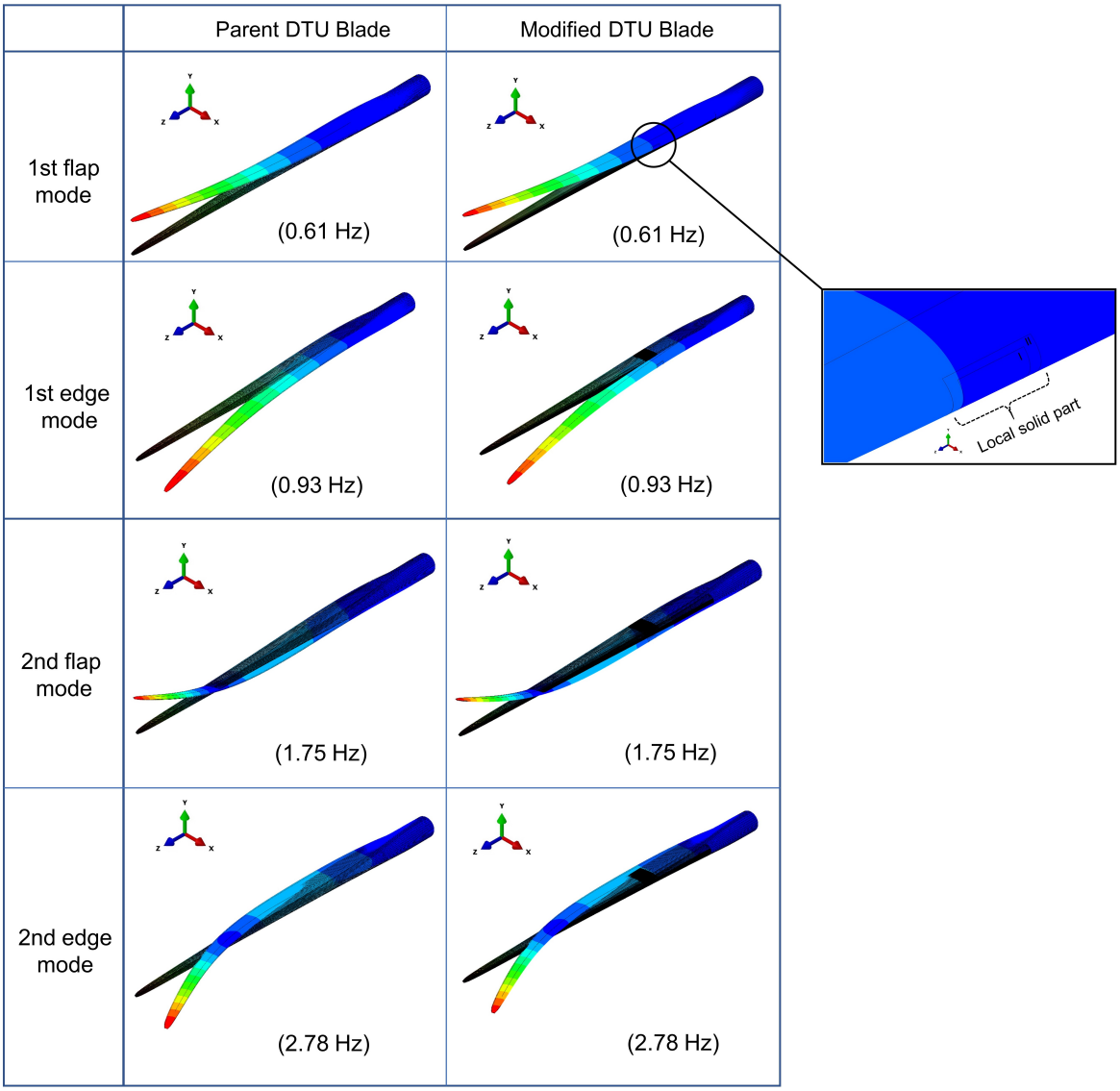

Figure 14: Comparison of global stiffness between modified and parent blade

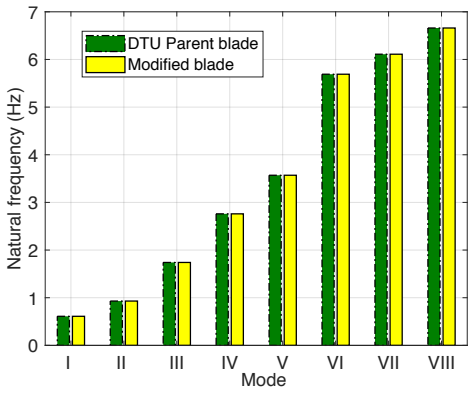

Figure 15: Comparison of global eigen frequencies between modified and parent blade

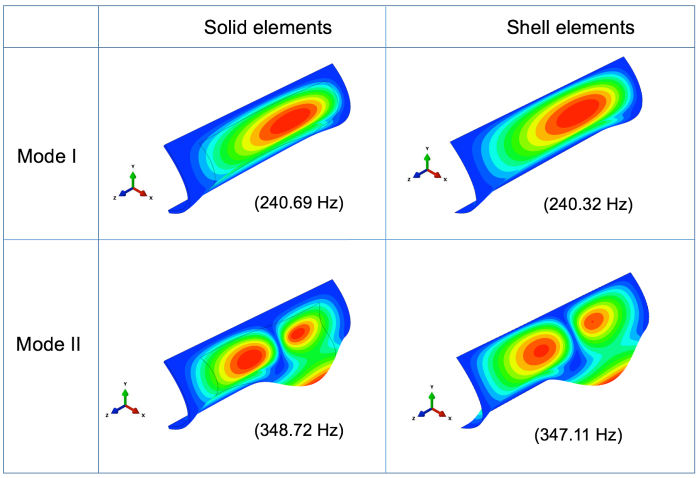

Figure 16: Comparison of local eigen frequencies for local solid part with solid and shell elements

discretised with different element types. Therefore, the eigenfrequency analysis is also conducted to compare between the leading edge section modelled with shell elements and that modelled with solid elements. These metrics also indicate a strong match, as shown in Fig. 16, where the eigenfrequencies and fringe plots for the corresponding first and second modes are presented. This confirms that the stiffness of the undamaged leading edge section is equivalent for different element types and thus that their impact responses can be compared.

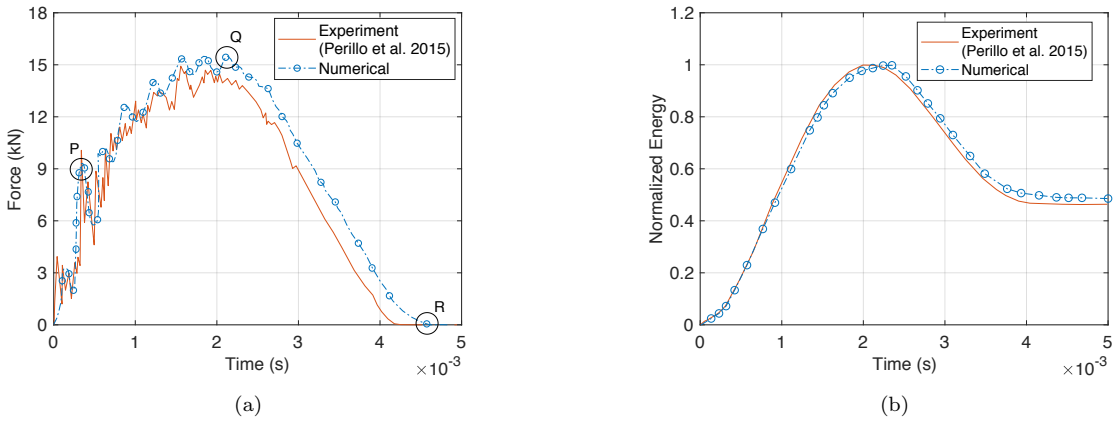

(a) (b)

Figure 17: Experiment and numerical curve (a) Contact force history comparison (b) Energy history comparison

B1. Validation of the implemented VUMAT subroutine

A user material VUMAT subroutine based on the Hashin failure criterion and compatible with solid brick elements is implemented in Abaqus/Explicit to progressively model the intraply damage modes in the laminate face sheets. To validate the accuracy of the subroutine, an experiment from the literature is taken, for which the impact modelling procedure with stacking sequence $[0/90/90/0]_s$ was discussed in section 4. Fig. 17(a) shows the comparison between the numerical and experimental contact force history curves (from [23]) for a case where an impactor hits the laminate with an impact velocity of 4.25 m/s (equivalent impact energy: 45.5 J). Note that

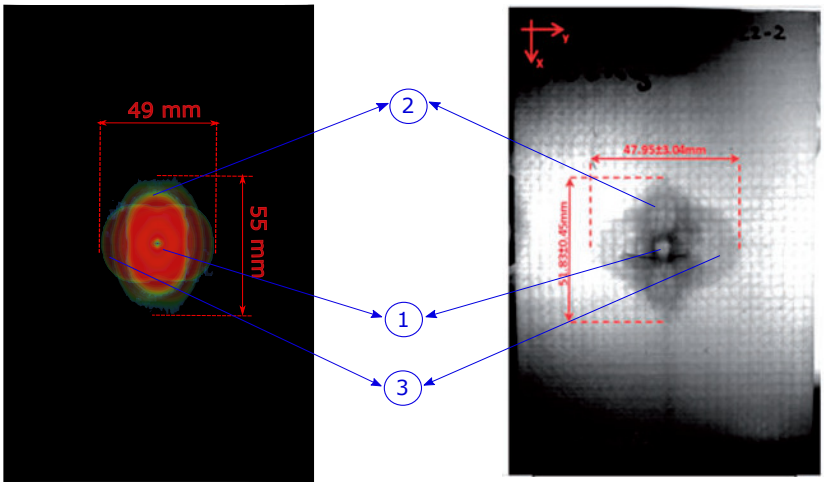

(a) *Left*: Numerical study *Right*: Experiment work [24]

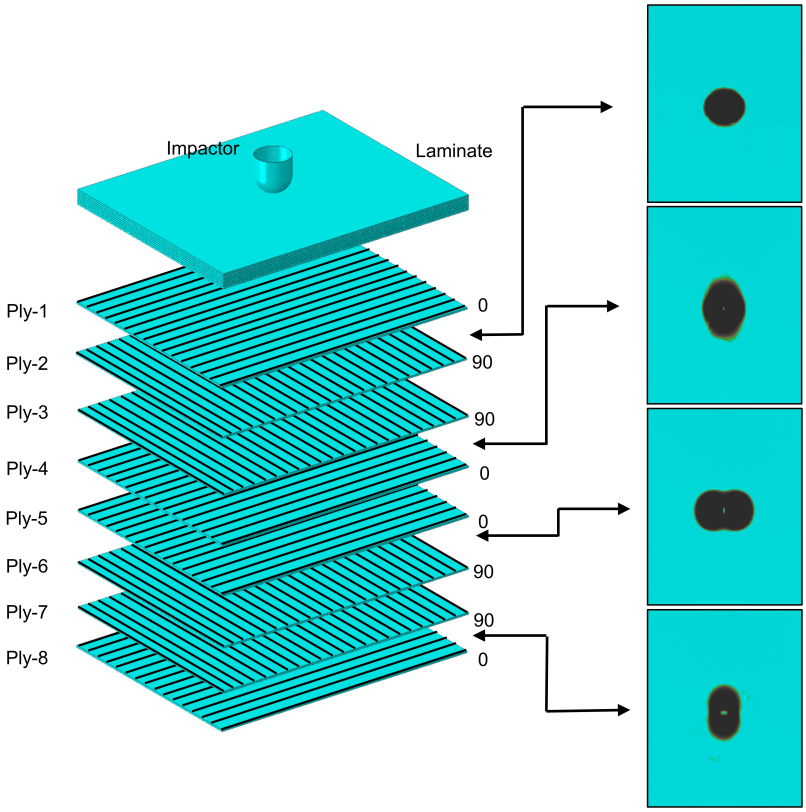

(b)

Figure 18: (a) Overall delamination shape and area comparison from numerical study and experiment from [24] (b) Delamination obtained at individual ply interfaces

the numerical contact force history presented here is filtered by separating the signal from its high-frequency components, which corresponds to non-physical numerical oscillations. From Fig. 17(a), good accordance between the contact force curves, including a satisfactory estimation of the threshold value (P) and the maximum value (Q) of the contact force, is seen; however, the numerical analysis predicts a slightly longer contact duration (R)

compared with that observed in the experiment. This outcome generally results from the additional time taken during the numerical procedure to release the contact between the impactor and the specimen compared with that in the experiment. Nevertheless, in general, the contact force history curves obtained numerically show an acceptable agreement with the experiment. A similar trend, showing concurrence in the estimated normalized absorbed energy history curves of the numerical and experimental results, can also be seen in Fig. 17(b). These results confirm that the numerical model with the implemented subroutine offers good concordance in assessing the impact responses.

Furthermore, the damages obtained from the numerical analysis and experimental study of [24] can also be compared, as shown in Fig. 18(a), where the delamination area in the laminate due to impact is presented. Note that the back-light technique was performed in the experiment (on the right side of Fig. 18(a)) to scan for damage that developed in the laminate due to impact. Thus, the overall delamination area is categorised at the laminate level and not at the individual ply interfaces. As a result, for comparison, Fig. 18(a) presents an envelope view of the superimposed delamination shapes from the numerical analysis, clearly showing a good comparison with the experiment (see portions marked with 1, 2 and 3 in Fig. 18(a)). Moreover, classical peanut shapes of the delamination were well captured in the numerical analysis. Fig. 18(b) presents the delamination shapes at the individual ply interfaces of the laminate. Clearly, the peanut shapes describing the delamination region are well represented and aligned in the direction of the fibre orientations. All in all, the implemented subroutine is found to estimate good results in accordance with those of the experiment, both in terms of impact response and damage evaluation, and thus is further utilised to study the wind turbine blade.

C. Impact investigation of wind turbine blade

The results for impact investigation on a wind turbine blade for a case where an impactor hits the leading edge are discussed here. Three distinct velocities of impact: 2 m/s, 3 m/s and 4 m/s and impact modelling techniques based on (1) pure shell, (2) shell-to-solid coupling, and (3) submodelling are considered. Note that the first part of the discussion is the comparison of impact responses in the blade describing contact forces, energies and displacement's histories obtained for each of the modelling techniques. A brief description of the validity of the numerical results based on mesh convergence study and examination of energy output histories are also made. Finally, the results for damage evaluation in the blade along with the overall computational analysis time involved for each modelling technique are compared.

Validation of numerical results: Mesh convergence study and examination of energy output history

To obtain numerically consistent and reliable results that are independent of mesh size effects, mesh convergence analyses are performed on the numerical models of the blade utilised in different modelling techniques. Different element sizes in the region of impact with dimensions varying as follows: 50 mm, 30 mm, 15 mm, 10 mm, 7.5 mm, 5 mm and 2.5 mm, are considered for the S4R elements utilised in the (1) shell-element-based technique and for the C3D8R elements utilised in the (2) shell-to-solid coupling and (3) submodelling techniques. The maximum contact force is chosen as the controlling parameter. Fig. 19(a) presents the mesh sensitivity results for a case where an impactor hits the leading edge with an impact velocity of 4 m/s. It can clearly be seen that the S4R shell element with a size of 10 mm used in the shell-based modelling technique gives consistent results for the contact forces, whereas C3D8R brick elements with a size of 5 mm used in the shell-to-solid coupling and submodelling techniques

give coherent results. In our study, however, a consistent element size of 5 mm for the shell as well as solid elements in the contact region for different techniques are chosen since one of the conditions is to compare the computational efficiencies. This ensures that the computational gain in the analysis time is not due to the presence of coarser meshes in the models but due to the kinematics of the different techniques utilised for impact investigation. Note that the different techniques, especially the shell-based approach, predict varying maximum contact forces, as seen in Fig. 19(a). This will be discussed in more detail in the subsequent discussions, where the impact responses are compared.

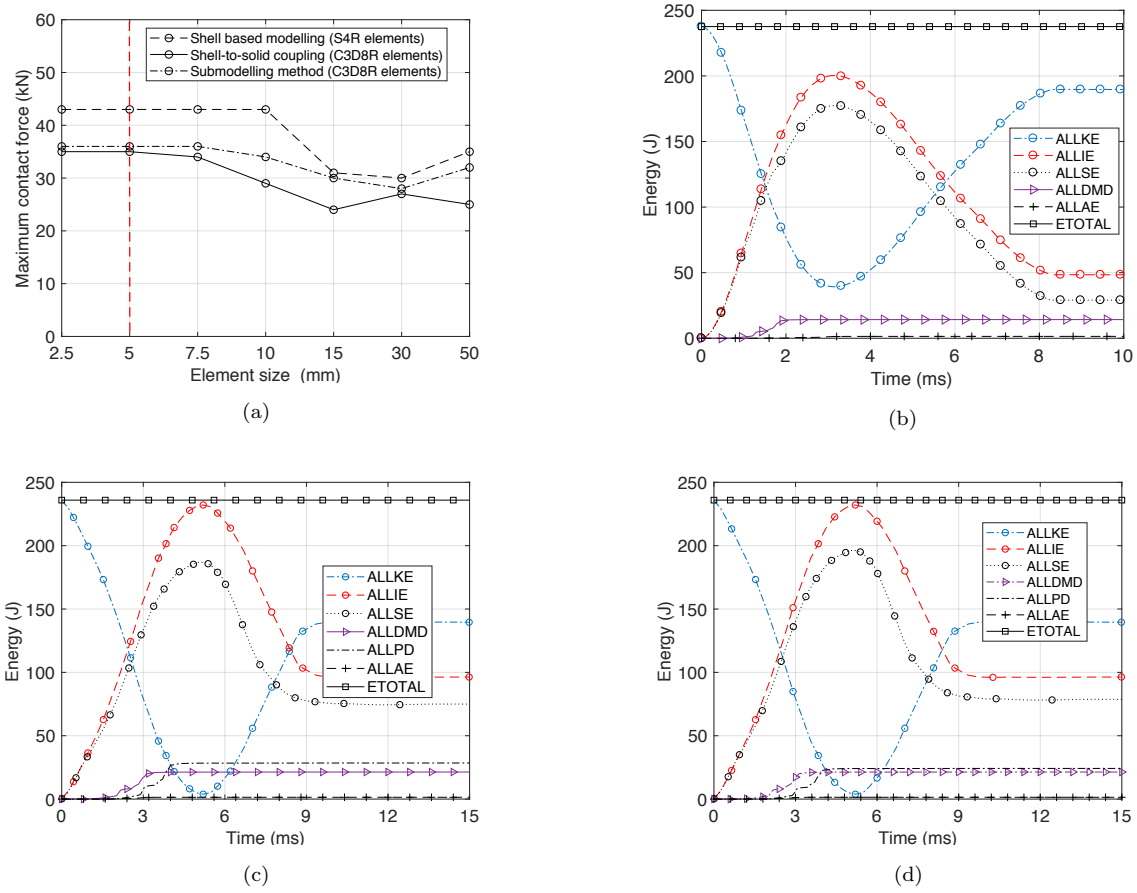

Figure 19: (a) Mesh convergence study ($V_x = 4$ m/s); Energy evolution history comparison between (b) pure shell (c) shell-to-solid coupling (d) submodelling technique for $V_x = 4$ m/s

Following the mesh convergence study, the energy output histories obtained from impact analyses of the blade using each of the modelling techniques are examined. This process is carried out to validate the numerical model's suitability as a result of applying the explicit-algorithm-based finite element solver in the study, which is conditionally stable. Figs. 19(b)-(d) present the evolutions of different energies for the (1) pure shell, (2) shell-to-solid coupling, and (3) submodelling techniques, respectively, for the case where an impactor hits the leading edge of the blade with an impact velocity of 4 m/s. Clearly, for all the modelling techniques, the total energy (ETOTAL) in the simulation remains constant (240 J); moreover, at any time step of the simulation, ETOTAL corresponds to the sum of the internal energy (ALLIE) and kinetic energy (ALLKE). This confirms the theory of energy conservation in the

numerical model. Furthermore, the internal energy (ALLIE) that develops in the blade due to impact overlaps with the elastic recoverable strain energy (ALLSE) during the initial phase of contact; however, after the development of damage energy (ALLDMD), the difference between the ALLIE and ALLSE is explicit. This indicates that some of the internal energy that develops in the blade is dissipated as damage in the form of failure modes. Moreover, the artificial strain energy (ALLAE), which is used in the numerical analysis to prevent any hourglass effects, is found to be less than 1% of the total energy for all the modelling techniques. Overall, the results confirm that the numerical model gives stable solutions.

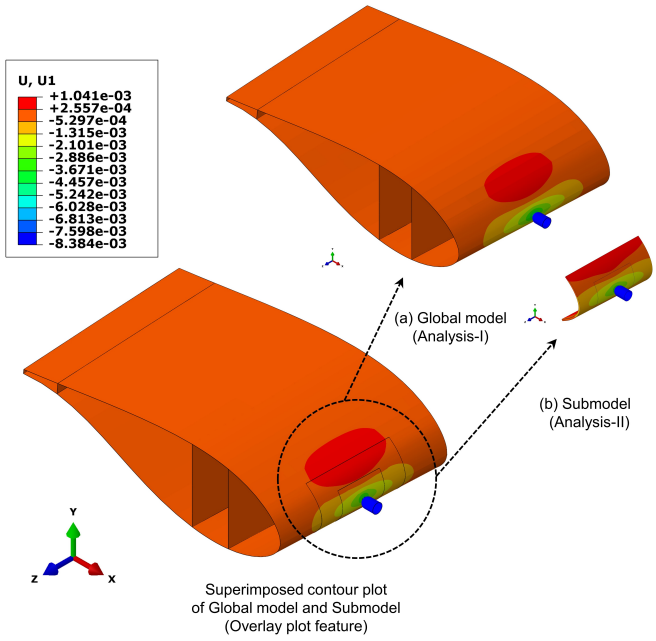

Figure 20: Displacement field equivalency between global model and submodel ($V_x = 4$ m/s)

Displacement field equivalency between global model and submodel

The (3) submodelling technique utilised in this study is based on a multistep analysis. The temporal displacement fields obtained based on calculation from shell elements (i.e. global analyis) are transferred as a boundary condition on the boundaries of the high-fidelity local submodel. Therefore, one of the most important items to check is whether these displacement fields are correctly mapped onto the driven nodes of the submodel and satisfy the displacement field equivalency requirements. Fig. 20 presents the appended contour plot for the displacement field on the overlapped global and local submodels where the impactor hits the leading-edge with $V_x = 4$ m/s. Strong accordance can be observed in the figure in which these displacement fields are accurately mapped. This can be further confirmed from Fig. 20(a) and 20(b), where the displacement fields captured in the global model and local submodel are separately illustrated for lucidity. The presented results affirm that the displacement boundary conditions are consistently transferred from the global analysis and that the submodelling technique gives stable results during impact investigations.

C1. Impact response study: Comparison between different techniques

The contact forces, out-of-plane displacement-time histories and energies obtained by the different modelling techniques during the impact investigation of a wind turbine blade for the case where the impactor hits its leading edge are compared. The results are discussed for all three impact velocities, i.e., 2 m/s, 3 m/s and 4 m/s, which correspond to impact energies of 60 J, 135 J and 240 J, respectively.

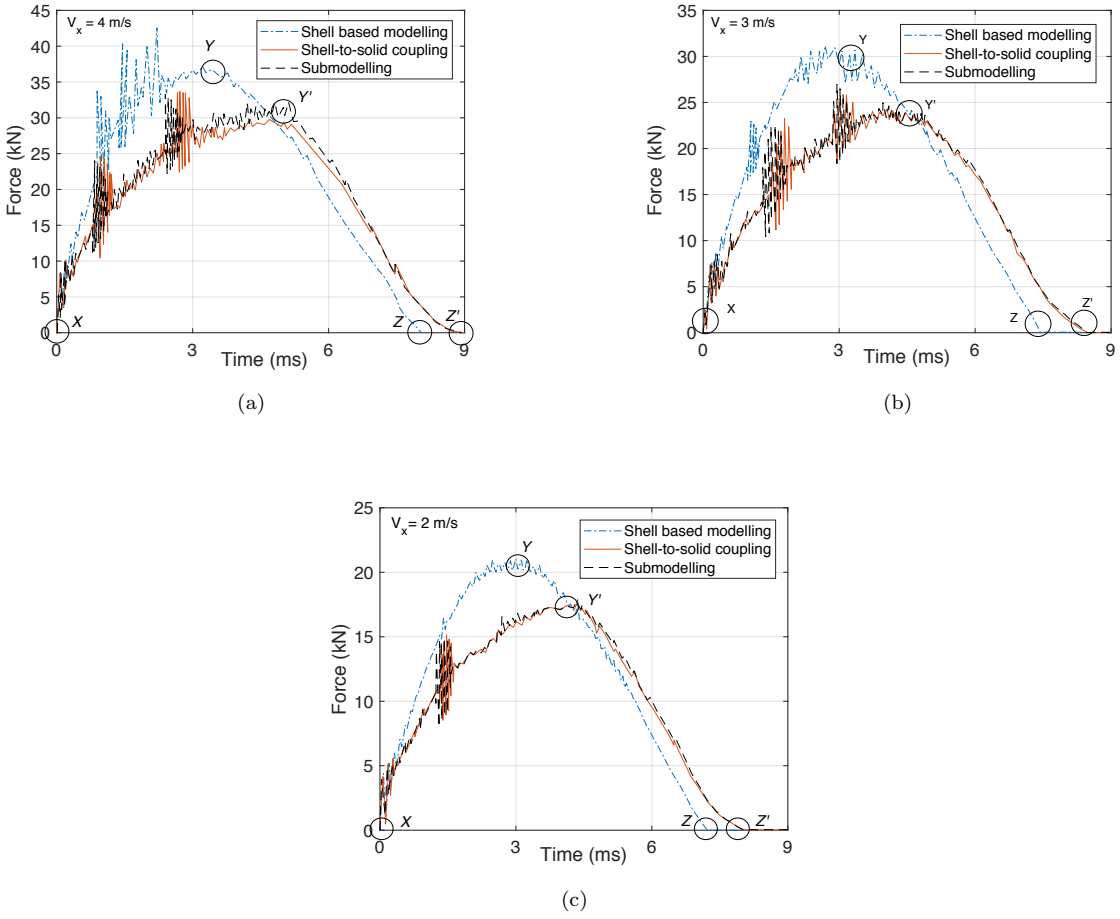

Figure 21: Contact force history comparison between modelling techniques for V_x = (a) 4 m/s (b) 3 m/s (c) 2 m/s (X: initiation of contact, Y: maximum deflection and impactor starts to rebound, Z: contact ends)

Figs. 21(a)-(c) present the contact-force history comparison for impact modelling based on the (1) pure shell, (2) shell-to-solid coupling, and (3) submodelling techniques for a case where an impactor hits the leading edge at impact speeds of 4 m/s, 3 m/s and 2 m/s, respectively. It can clearly be seen from all the curves that the (1) shell-based model estimates a larger contact force (denoted by '*Y*' in Figs. 21(a), (b) and (c)) and a relatively shorter contact duration ('*Z*') compared to those of the other two global-local techniques (*Y*',*Z*'). On the other hand, the (2) shell-to-solid coupling and (3) submodelling techniques predict quite similar results for the contact force evolution and contact duration. This difference in impact response prediction for different element types is attributed to the different kinematics of the failure mode predictions for shell and solid elements, with the former behaving more stiffly compared to the solid elements and overestimating the impact responses.

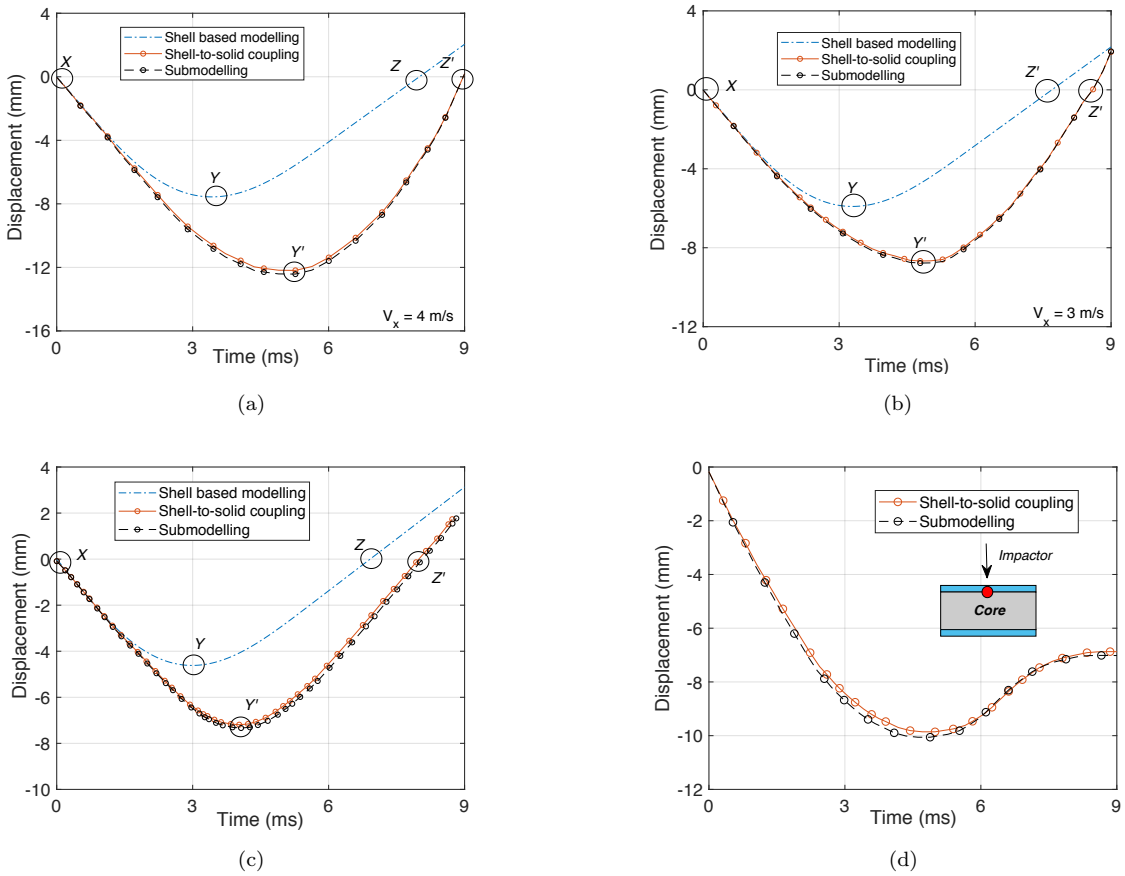

Figure 22: Displacement history comparison for impactor between modelling techniques for V_x = (a) 4 m/s (b) 3m/s (c) 2m/s (d) Comparison for displacement predicted on the outer layer of the core by global-local methods (X: initiation of contact, Y: maximum deflection and impactor starts to rebound, Z: contact ends)

Figs. 22(a)-(c) present the comparison between displacement-time histories of the impactor predicted by different modelling techniques for impact velocities of 4 m/s, 3 m/s and 2 m/s, respectively. From the figures, it can be reaffirmed that the (1) shell-element-based modelling approach presents a stiffer response and thus allows less displacement of the impactor (Y) compared to other techniques; on the other hand, the (2) shell-to-solid coupling and (3) submodelling techniques based on solid elements present more compliant responses to the impactor and predict almost similar impact response results. The large displacements of the impactor calculated by the (2) shell-to-solid coupling and (3) submodelling techniques are attributed to the detailed failure modes, e.g., crushing and plastic deformation of the core, being correctly modelled using solid elements. Fig. 22(d) presents the displacement history of a node defined on the top layer of the core modelled with solid elements during impact, clearly showing the extent of permanent deformation of the core. A detailed comparison of the damage modes modelled by all three techniques will be discussed in the next section. Also, the displacement curves predicted by the different techniques initially overlap each other (Figs. 22(a)-(c)), which confirms that the shell and solid elements exhibit equivalency in stiffness during the early stages of impact before the development of damage.

Fig. 23 shows the comparison between recoverable elastic strain energy (ALLSE) and permanently absorbed

energy levels (sum of ALLPD and ALLDMD) predicted by the different techniques for three different impact velocities: 2 m/s, 3 m/s and 4 m/s. For all the impact velocities, the (1) shell-based modelling technique underpredicts the permanently absorbed energy in the numerical model compared to the (2) shell-to-solid coupling and (3) submodelling techniques. Again, this is attributed to the failure mode prediction capabilities of solid elements over shell elements, where detailed failure modes such as delamination and plastic deformations are captured. Note that for all the cases, the ratio of permanently absorbed energy (sum of ALLPD and ALLDMD) to elastic strain energy (ALLSE) ranges between 2% - 30% of the total internal energy that develops in the blade due to impact. This implies that most of the energy due to impact is absorbed as elastic energy, with less energy dissipated in the form of damage or inelastic deformation. This result reaffirms the requirement for considering the flexibility of the entire composite structure during impact analysis.

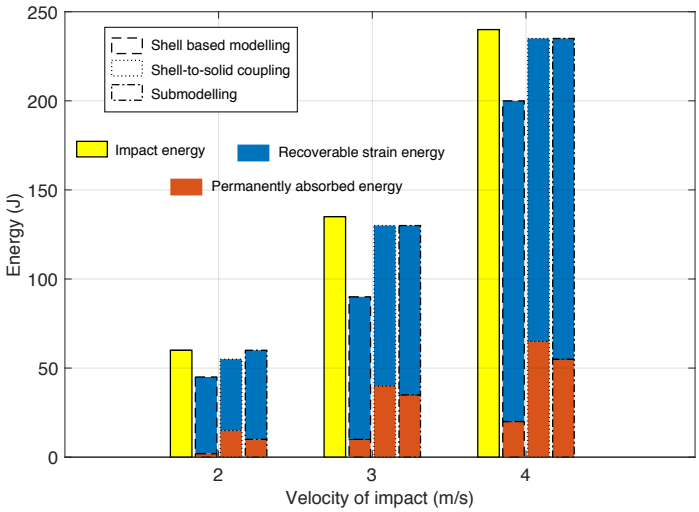

Figure 23: Comparison of permanently absorbed and elastic strain energy modelled with different techniques

C1. Damage evaluation study: Comparison between different techniques

The results of the damage evaluation of the blade for the case where an impactor hits its leading edge with an impact velocity of 4 m/s and those predicted by the different modelling techniques are discussed and compared here. Note that the leading edge is a sandwich section with two different materials; thus the failure modes predicted for the top and bottom laminate face sheets are described. Finally, the damages predicted exclusively for the core are presented.

Figs. 24, 25 and 26 present the intralaminar failure modes developed in the GFRP laminate face sheets predicted by the (1) pure shell, (2) shell-to-solid coupling, and (3) submodelling techniques, respectively. For the (1) pure-shell-element-based approach, the post-impact final damage state of the middle-most section for each ply (except for Ply-5, which corresponds to the core), predicted based on the Hashin 2D failure criterion, is presented in Fig. 24. Clearly, this modelling method predicts failure in all the plies through the thickness; most of the plies in the laminate closer to the impact surface fail by matrix compression (DAMAGEMC), whereas the plies away from the impactor on the other side of the core fail by matrix tensile failure modes (DAMAGEMT). Note that these

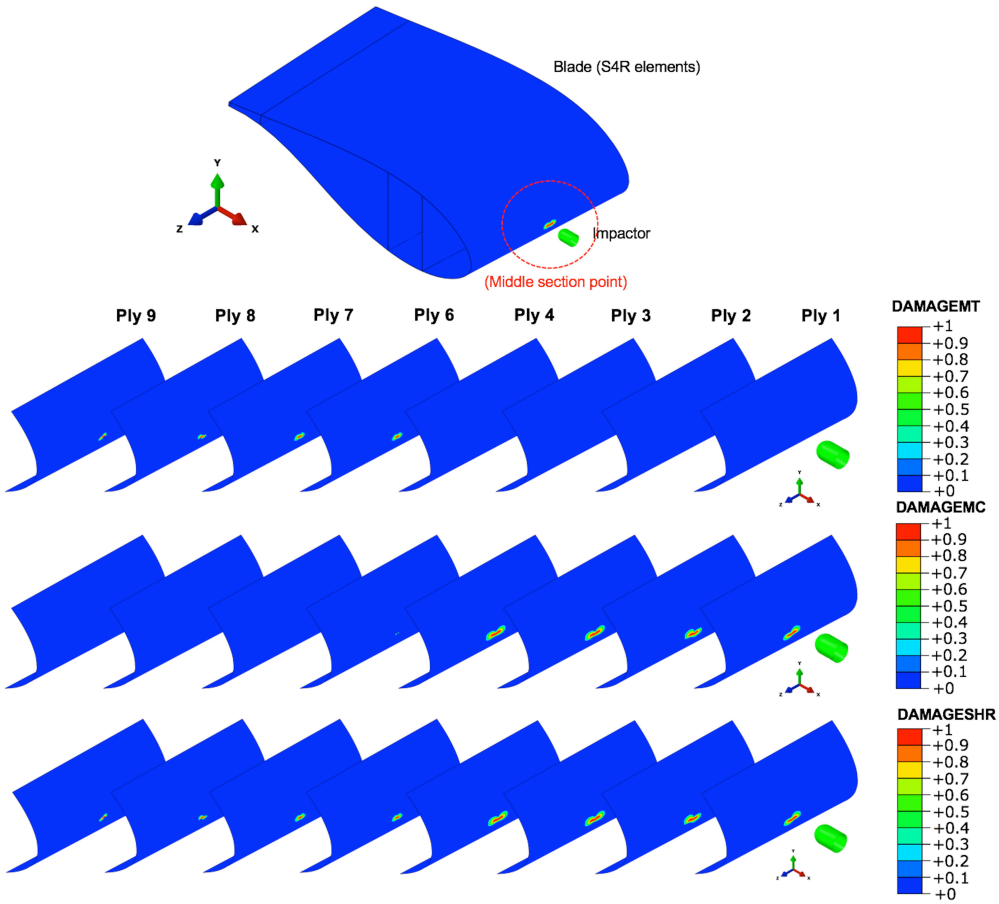

Figure 24: Intralaminar failure modes predicted based on (1) pure shell based method for V_x=4 m/s

mostly correspond to the flexural type of failure modes that develops in the leading edge section due to transverse impact. Again, the shear damage (DAMAGESHR) predicted by the Hashin 2D failure criterion, which considers the interaction between all failure modes, predicts the failure in all the plies through the thickness. However, despite all the plies failing in matrix-dominated failure modes, there is no element deletion in the finite element model owing to the formulation of shell elements, where the elements are deleted only if all the section integration points in an element through the thickness satisfy the failure criteria. Since no fibre failure modes were obtained for the plies, the elements were consequently not deleted. This implies that the (1) pure-shell-based method cannot capture any impact-induced surface eroding effects in a blade. This failure mode is important to model from the leading edge perspective, as this could hinder the smooth flow of wind through the aerodynamic profile, thus affecting the aerodynamic performance of the blade. Furthermore, there were no indentations in the laminate face sheets due to impact based on the (1) pure-shell-based modelling technique. Thus, any failure mode in the top plies due to impact-induced local deformations were not predicted. This is an important failure mode found in a sandwich section, where the top face sheet suffers from matrix fracture and local indentation due to local contact forces. This limitation of the shell-based method is important, as three-dimensional stresses are not considered while examining damage responses. Furthermore, delamination in the laminate face sheets, which is one of the most critical failure modes due to impact, was not modelled and predicted using this approach.

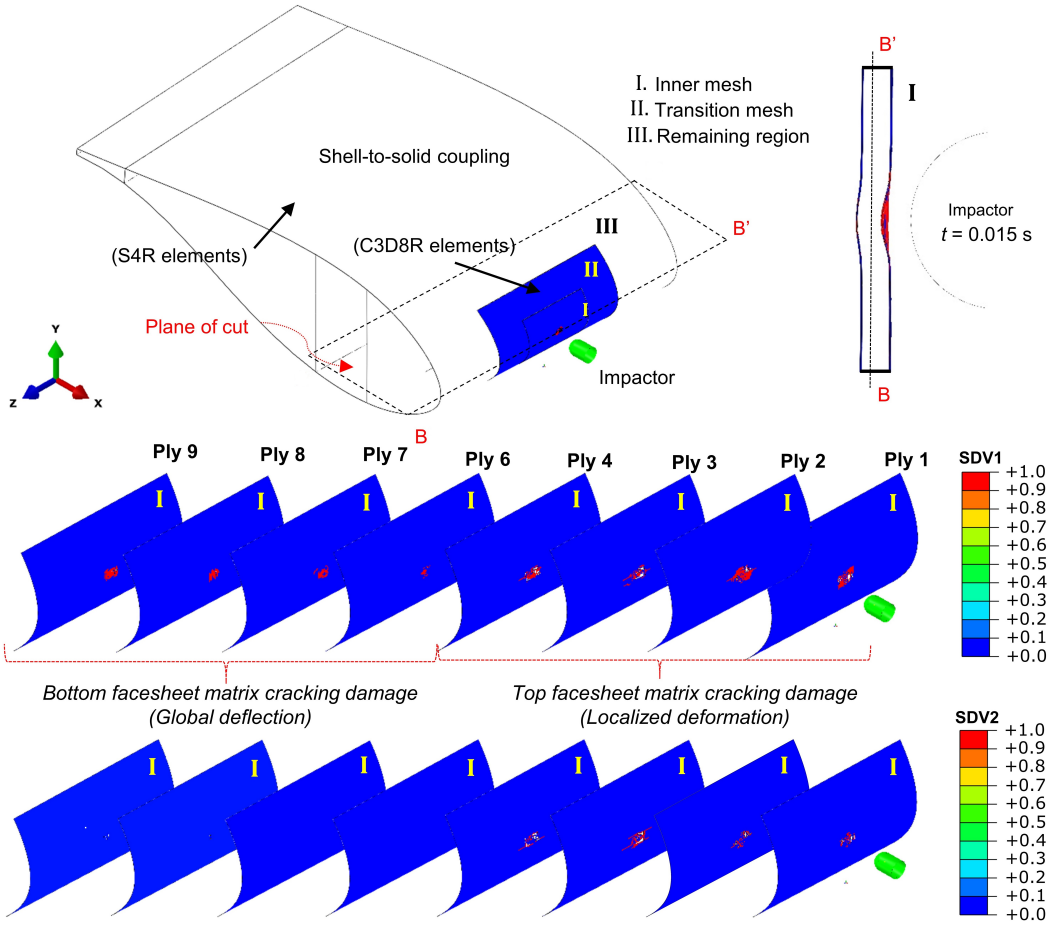

Figure 25: Intralaminar failure modes predicted based on (2) shell-to-solid coupling method for V_x=4 m/s

In contrast, the (2) shell-to-solid coupling and (3) submodelling methods clearly capture the localized deformations in the top face sheets and corresponding associated matrix cracking failure modes and local indentation, as can be seen through a section cut (BB') in Figs. 25 and 26. In addition, the failure modes in the plies based on flexural effects are also well predicted, with the top plies failing under matrix compression (SDV2) and the plies at the bottom face sheet failing under matrix tensile failure modes (SDV1). The (2) shell-to-solid coupling and (3) submodelling methods also predict delaminations at the ply interfaces, which are mostly concentrated in the top face sheets; however, a few plies below the core also exhibit delamination (delamination footprints presented in red in Fig. 28). Furthermore, the implemented VUMAT subroutine was defined with a variable 'STATUS', which enables the solid elements to be deleted even if any of the failure modes in the plies are predicted. Overall, it looks like the global-local methods, i.e., the (2) shell-to-solid coupling and (3) submodelling methods based on solid elements, predict comprehensively almost all the failure modes in the laminate face sheets compared to the (1) shell-based method. Moreover, these predictions based on the global-local methods are quite similar to each other.

In addition to the failure modes discussed for the laminate face sheets, there are at least three other failure modes in a sandwich section due to the presence of the core. These are as follows: core shear failure, core crushing and face-core debonding. Note that this discussion is restricted to non-perforated damage in the sandwich structure.

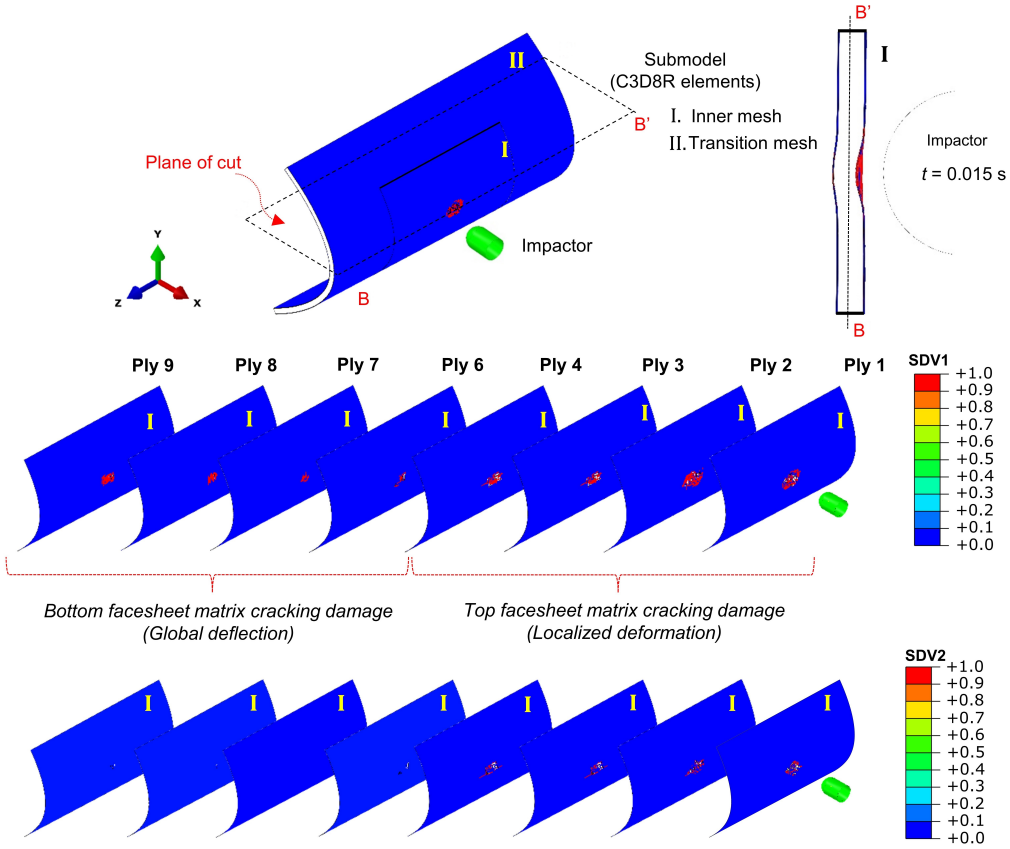

Figure 26: Intralaminar failure modes predicted based on (3) submodelling method for V_x=4 m/s

The transverse core shear failure in a sandwich section is predicted when the transverse shear stresses (τ_{13}, τ_{23}) in the core exceed their critical transverse shear strength values. The variation of these stresses (τ_{13}, τ_{23}) in the (1) shell-element-based approach are not considered in the element formulation explicitly but are post-processed at

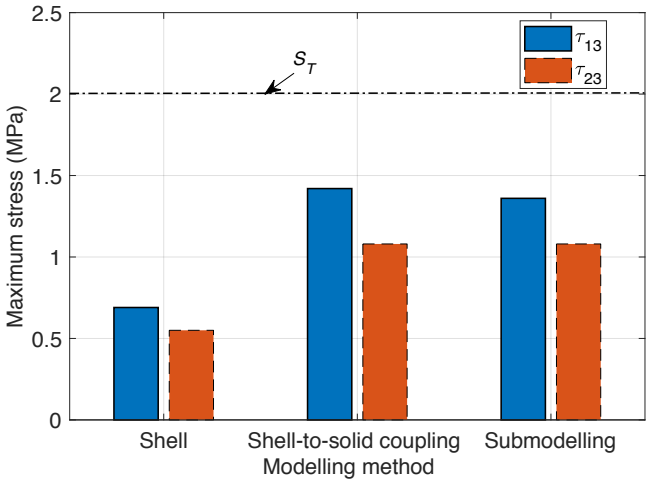

Figure 27: Comparison of maximum transverse shear stresses predicted in the core based on different techniques

suitable section points as output variables denoted by TSHR13 and TSHR23, respectively. This is implemented for thick shell elements in Abaqus (S4R elements utilised in this study), where the stresses are evaluated by mapping the elastic strain energy corresponding to the shear deformation of the shell section with a parabolic variation of the shear stresses together with the correction factors [30, 48]. On the other hand, the (2) shell-to-solid coupling and (3) submodelling techniques, which are based on solid elements, consider these stresses explicitly in their formulation and give more reliable predictions of the transverse shear stresses in the core. Fig. 27 presents the impact-induced maximum transverse shear stresses predicted in the core (τ_{13}, τ_{23}) by the (1) pure shell, (2) shell-to-solid coupling, and (3) submodelling techniques. It can be seen that the maximum transverse shear stresses predicted by all the methods are less than the transverse shear strength value of the core (2 MPa). This observation suggests that the shear failure in the core was not predicted by any of the methods. Nevertheless, the shell elements still underpredict these critical stresses compared to solid elements. Furthermore, the (1) pure-shell-element-based method does not consider out-of-plane transverse normal stresses and thus cannot capture core crushing effects causing permanent deformation in the core. On the other hand, these were clearly well predicted using the (2) shell-to-solid coupling

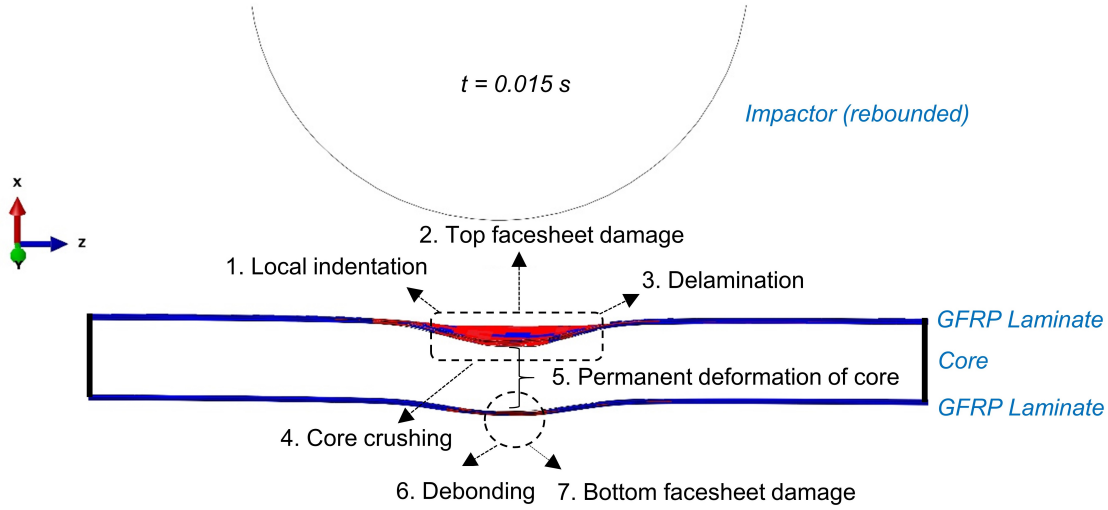

Figure 28: Failure modes modelled at the leading edge using global-local methods (*viewed at BB' plane of cut*)

and (3) submodelling techniques, as can be seen in Figs. 25 and 26, respectively, where a cross-sectional view in the BB' plane of a cut is shown. These are also explicitly shown in Fig. 28, where the cut BB' in the region of impact is enlarged. It is also worth mentioning that the face-core debonding was also captured at the interface of the face and bottom core by the global-local modelling methods based on solid elements, whereas shell elements could not capture it. Finally, Fig. 28 illustrates important failure modes predicted in the leading edge (here, the sandwich section) by the global-local methods, i.e., the (2) shell-to-solid coupling and (3) submodelling techniques.

Summary of modelling capabilities of different techniques

Table 5 summarizes the capabilities of the modelling techniques in predicting different failure modes for the case where an impactor hits the leading edge (here, a sandwich section). The shell-based modelling technique can only capture face sheet damage related to the flexural failure modes as well as predict core shear failure. Note that

the core shear failure is not modelled explicitly but is predicted based on output variables TSHR13 and TSHR23 implemented for a thick shell; however, it underpredicts these stresses, and the accuracy is limited. Other failure modes such as the local surface indentation, face sheet damage due to local deformations, delamination, surface eroding, core crushing and face core debonding were not modelled by the (1) pure-shell-based approach. On the other hand, the (2) shell-to-solid coupling and (3) submodelling methods, which utilise solid elements in the local region, were capable of explicitly modelling all the major failure modes, with their results being similar.

Table 5: Modelling capabilities of different techniques

S.No	Damage modes	**Pure shell**	**Shell-to-solid coupling**	**Submodelling**
1	Local indentation	N	Y	Y
2	Face sheet damage	Y[a]	Y	Y
3	Delamination	N	Y	Y
4	Eroding of surface	N	Y	Y
5	Core crushing	N	Y	Y
6	Core shear failure	Y[b]	Y[b]	Y[b]
7	Debonding	N	Y	Y

a- *only flexural-type failure mode*; b- *not modelled but predicted*; (Y:Yes, N: No)

Comparison of computational analysis durations for different techniques

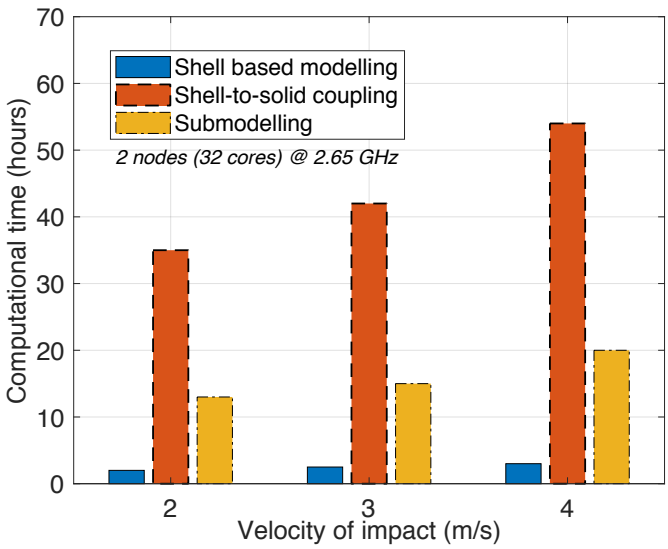

Figure 29: Comparison of computational analysis time based on different techniques

The overall computational analysis durations of the (1) pure shell, (2) shell-to-solid coupling, and (3) submodelling techniques for different cases of impact velocities are compared. The analyses were run on an high performance computing (HPC) machine with a cluster of two nodes and a total of 32 cores, with a processor speed

of 2.65 GHz. Fig. 29 clearly shows that the (1) shell-based modelling technique is the cheapest analysis among the three modelling techniques. Nevertheless, the technique is limited in accuracy for impact investigation, as it could not capture important failure modes in the blade. On the other hand, the global-local methods, i.e., the (2) shell-to-solid coupling and (3) submodelling techniques, capture similar impact responses and damage evolution in the blade. However, the (2) shell-to-solid coupling technique requires almost twice the computational time needed for the (3) submodelling technique; the longer time taken by the (2) shell-to-solid coupling technique is attributed to the highly stable time increment required for the elements in the region of shell-to-solid coupling between the shell and transition regions of the local model. Note that the (3) submodelling technique is based on a multistep analysis and thus that the results presented here include the total time for global analysis based on shell elements together with the time required to carry out the local submodel analysis. Overall, the (3) submodelling-based impact modelling technique is found to be the most efficient analysis for the case considered in our study.

7. Conclusions

The present study evaluated different numerical modelling techniques for the impact investigation of a wind turbine blade for a case where an impactor hits the leading edge. The importance of the numerical analysis considering the full-scale length of the structure was emphasized. It was mentioned that a realistic composite structure such as a wind turbine blade, compared to its coupon-scale representation, has large flexibility with complex boundary conditions; thus, the entire elastic response, inertia and realistic boundary conditions need to included in the finite element model to correctly model the impact dynamics. The primary objective of the paper was to study modelling technique alternatives to a completely brick-element-based formulation of the entire structure, which is not attractive to industry owing to the high computational cost involved. Therefore, three existing techniques in Abaqus, i.e., the (1) pure shell technique and global-local methods based on (2) shell-to-solid coupling, and (3) submodelling, were compared.

The DTU 10 MW blade based on shell elements was chosen as the reference blade in this study, for which the high-fidelity local solid part of the leading edge in the region of impact was developed in the first part of the paper. The goal was to use this as the 'local' solid finite element model in the global-local methods. The stiffness characteristics of the modified blade were compared with the baseline to validate the modelling equivalency, revealing a strong match at both the global and local sectional levels. Also, a user material VUMAT subroutine was implemented in Abaqus for modelling intralaminar failure modes in the composite laminates, for which the accuracy and validity of the subroutine were compared with those observed in an experiment from the published literature. The subroutine predicted good results for impact responses and damage evaluation and was utilised further for impact investigation of the blade. The main findings of the impact investigation of a wind turbine blade based on different modelling techniques are as follows:

1. For the comparison of the impact responses predicted by the different techniques, it is found that the (1) pure-shell-based modelling technique exhibits a stiffer response to the impact and predicts a higher maximum contact force and smaller contact duration. It further underestimates the out-of-plane displacement of the impactor as well as permanently absorbed energy levels developed in the blade due to impact. The (2) shell-to-solid coupling and

(3) submodelling methods, on the other hand, provide almost similar results for the contact forces, displacements, and energies and present a softer response, owing to its capability to predict detailed failure modes.

2. The energy results for the different modelling techniques reaffirm the understanding that a composite structure, owing to its large flexibility, absorbs a large part of the impact energy in the form of elastic strain energy, with only 2% - 30% of the energy dissipated as permanently absorbed energy in the form of damages and inelastic deformations.

3. For the comparison of the impact-induced-damage evaluations of the leading edge based on different techniques, it is found that the (1) pure-shell-based method's ability to predict failure modes due to impact on the blade at its leading edge (here, for a sandwich section) is limited. The method predicts the flexural failure mode in the laminate face sheet upon impact; however, the damage due to local deformations is not captured. Furthermore, surface indentations, impact-induced surface eroding effects, delamination, and failure modes such as core crushing and debonding are not modelled and predicted when using the shell-element-based approach. In contrast, the (2) shell-to-solid coupling and (3) submodelling methods are able to model and predict all major impact-induced failure modes, with the results being similar to each other.

4. The (3) submodelling method is the most efficient analysis technique, providing sound impact response and damage evaluation results much closer to those predicted by the (2) shell-to-solid coupling method but with half the computational expense. The shell-based modelling technique is by far the cheapest analysis among all the three techniques, although its accuracy for impact investigation is limited.

8. Limitations and future work

The present study is limited to a case where an impactor hits the leading edge of a fixed wind turbine blade. In the future, similar studies need to be conducted to compare modelling techniques in a situation where a blade with an initial velocity impacts a structure. Such a scenario is more realistic during offshore installations, where due to large motions, impact loads are anticipated in the lifted blade.

Further, other critical region in the wind turbine blade for example, trailing edges, and blade tip needs to be investigated, where the effect of delamination crack will have significant effect on the blade's structural integrity. Additionally, the damage modes modelled in the sandwich section in this study closely resembles those of previous studies. However, an experimental study will be needed to closely validate the models. Note that the leading edge considered in the study has a sandwich section which resembles the composition of an integrated blade with no adhesive connections. A generic blade consisting of adhesive joints at the leading edge should be addressed to understand the damage evaluation for such material combinations.

Also, from the finite element method perspective, in the current work, two most common global-local methods- (2) shell-to-solid coupling and (3) submodelling methods- were utilised to compare impact analysis of a wind turbine blade. These methods are widely applied in the industry and are made available in commercial FEM codes like Abaqus and Ansys [50]. However, it is to be noted that there exist other coupling or bridging techniques in the literature, such as Arlequin method [51], bridging domain method [52], and the s-version method [53] to name a few. These methods have shown to have a wide application and merits in terms of global-local techniques [54], where the analysts can have immense freedom to choose the scale of investigations [55]. Therefore, it would be

interesting to implement and compare these methods with the ones used in this study for impact investigation on a wind turbine blade. Further, it is worth mentioning that new finite element techniques and new codes from the existing finite element model must be developed in the future to solve these impact problems at hand.

9. Data Availability

The raw/processed data required to reproduce these findings cannot be shared at this time as the data also forms part of an ongoing study.

Acknowledgment

This work was made possible through the SFI MOVE projects supported by the Norwegian Research Council, NFR project number 237929. The authors would also like to thank uninett sigma2 for the computational hours on cluster. The authors would also like to thank anonymous reviewers for their valuable suggestions and comments that help to improve the quality of the work.

References

[1] L. Li, Dynamic Analysis of the Installation of Monopiles for Offshore Wind Turbines, PhD Thesis, Norwegian University of Science and Technology (NTNU), Trondheim (2016).

[2] A. S. Verma, Z. Jiang, N. P. Vedvik, Z. Gao, Z. Ren, Impact assessment of a wind turbine blade root during an offshore mating process, Under review in Engineering structures.

[3] A. Ho, A. Mbistova, G. Corbetta, The european offshore wind industry–key trends and statistics 2016, Report, The European Wind Energy Association (EWEA) (2017).

[4] A. Nghiem, I. Pineda, Wind energy in Europe: Scenarios for 2030, Wind Europe.

[5] S. Darius, GE unveils market–changing 12MW offshore wind turbine, `http://www.rechargenews.com/wind/1443296/ge-unveils-market-changing-12mw-offshore-wind-turbine` (Accessed: 2018-03-01).

[6] P. Haselbach, Ultimate Strength of Wind Turbine Blades under Multiaxial Loading, PhD Thesis, DTU Wind Energy (2015).

[7] P. Brøndsted, R. P. Nijssen, Advances in wind turbine blade design and materials, Elsevier, 2013.

[8] D. Feng, Simulation of low-velocity impact damage in sandwich composites, Ph.D. thesis, Universita'degli Studi di Cagliari (2014).

[9] A. S. Verma, P. U. Haselbach, N. P. Vedvik, Z. Gao, A Global-local damage assessment methodology for impact damage on offshore wind turbine blades during lifting operations (Accepted), 37th International Conference on Ocean, Offshore and Arctic Engineering OMAE (2018).

[10] P. J. Schubel, R. J. Crossley, Wind turbine blade design, Energies 5 (9) (2012) 3425–3449.

[11] A. S. Verma, N. P. Vedvik, Z. Gao, Comprehensive numerical investigation of impact behavior of an offshore wind turbine blade due to impact/contact during installation, Under review in Ocean Enginerring.

[12] S. Abrate, Impact on composite structures, Cambridge university press, 2005.

[13] S. Agrawal, K. K. Singh, P. Sarkar, Impact damage on fibre-reinforced polymer matrix composite–a review, Journal of Composite Materials 48 (3) (2014) 317–332.

[14] P. Haselbach, R. Bitsche, K. Branner, The effect of delaminations on local buckling in wind turbine blades, Renewable Energy 85 (2016) 295–305.

[15] D. N. Veritas, Design and manufacture of wind turbine blades, offshore and onshore wind turbines, DNV Standard, DNV-DS-J102 (2010) 2010–11.

[16] X. Zhang, Impact damage in composite aircraft structures–experimental testing and numerical simulation, Proceedings of the Institution of Mechanical Engineers 212 (4) (1998) 245.

[17] B. Hayman, Approaches to damage assessment and damage tolerance for frp sandwich structures, Journal of Sandwich Structures & Materials 9 (6) (2007) 571–596.

[18] M. McGugan, G. Pereira, B. F. Sørensen, H. Toftegaard, K. Branner, Damage tolerance and structural monitoring for wind turbine blades, Phil Trans R Soc A 373 (2035).

[19] A. Standard, D7136: Standard test method for measuring the damage resistance of a fiber-reinforced polymer matrix composite to a drop-weight impact event, ASTM International: West Conshohocken.

[20] B. Boeing, 7260, Advanced Composite Compression Tests, The Boeing Company, Seattle, WA.

[21] S. P. Rajbhandari, M. L. Scott, R. Thomson, D. Hachenberg, An approach to modelling and predicting impact damage in composite structures, ICAS Congress (2002) 8–13.

[22] G. Perillo, J. Jørgensen, Numerical/experimental study of the impact and compression after impact on gfrp composite for wind/marine applications, Procedia Engineering 167 (2016) 129–137.

[23] G. Perillo, J. K. Jørgensen, R. Cristiano, A. Riccio, A Numerical/Experimental Study on the Impact and CAI Behaviour of Glass Reinforced Compsite Plates, Applied Composite Materials 25 (2) (2018) 425–447.

[24] G. Perillo, N. Vedivik, A. Echtermeyer, Damage development in stitch bonded GFRP composite plates under low velocity impact: Experimental and numerical results, Journal of Composite Materials 49 (5) (2015) 601–615.

[25] X. Sun, S. Hallett, Barely visible impact damage in scaled composite laminates: Experiments and numerical simulations, International Journal of Impact Engineering 109 (2017) 178–195.

[26] L. Gigliotti, S. Pinho, Multiple length/time-scale simulation of localized damage in composite structures using a Mesh Superposition Technique, Composite Structures 121 (2015) 395–405.

[27] C. Lopes, P. Camanho, Z. Gürdal, P. Maimí, E. González, Low-velocity impact damage on dispersed stacking sequence laminates. Part II: Numerical simulations, Composites Science and Technology 69 (7-8) (2009) 937–947.

[28] S. Abrate, Criteria for yielding or failure of cellular materials, Journal of Sandwich Structures & Materials 10 (1) (2008) 5–51.

[29] J. N. Reddy, Mechanics of laminated composite plates and shells: theory and analysis, CRC press, 2004.

[30] H. Hibbitt, B. Karlsson, P. Sorensen, Abaqus analysis users manual version 2016.

[31] M. Nachtane, M. Tarfaoui, A. El Moumen, D. Saifaoui, Damage prediction of horizontal axis marine current turbines under hydrodynamic, hydrostatic and impacts loads, Composite Structures 170 (2017) 146–157.

[32] Z. Hashin, Failure criteria for unidirectional fiber composites, Journal of applied mechanics 47 (2) (1980) 329–334.

[33] I. Lapczyk, J. A. Hurtado, Progressive damage modeling in fiber-reinforced materials, Composites Part A: Applied Science and Manufacturing 38 (11) (2007) 2333–2341.

[34] N. Nanami, O. Ochoa, Bird impact study of a preloaded composite wind turbine blade, energy 15 (2013) 2.

[35] M. Peeters, G. Santo, J. Degroote, W. Van Paepegem, Comparison of Shell and Solid Finite Element Models for the Static Certification Tests of a 43 m Wind Turbine Blade, Energies 11 (6) (2018) 1346.

[36] R. Gibbon, L. Vaughn, Using Different Modelling Techniques for the Simulation of Impact upon Composites for Aerospace Applications, Presented at Innovation in Composites.

[37] S. Hühne, J. Reinoso, E. Jansen, R. Rolfes, A two-way loose coupling procedure for investigating the buckling and damage behaviour of stiffened composite panels, Composite Structures 136 (2016) 513–525.

[38] M. Akterskaia, E. Jansen, S. Hühne, R. Rolfes, Efficient progressive failure analysis of multi-stringer stiffened composite panels through a two-way loose coupling global-local approach, Composite Structures 183 (2018) 137–145.

[39] Z. Nie, Advanced mesomechanical modeling of triaxially braided composites for dynamic impact analysis with failure, PhD Thesis, The University of Akron (2014).

[40] J. Reinoso, A. Blázquez, A. Estefani, F. París, J. Cañas, E. Arévalo, F. Cruz, Experimental and three-dimensional global-local finite element analysis of a composite component including degradation process at the interfaces, Composites Part B: Engineering 43 (4) (2012) 1929–1942.

[41] O. R. Shah, M. Tarfaoui, The identification of structurally sensitive zones subject to failure in a wind turbine blade using nodal displacement based finite element sub-modeling, Renewable Energy 87 (2016) 168–181.

[42] L. Sutherland, A review of impact testing on marine composite materials: Part I–Marine impacts on marine composites, Composite Structures.

[43] C. Bak, F. Zahle, R. Bitsche, T. Kim, A. Yde, L. C. Henriksen, M. H. Hansen, A. Natarajan, Description of the DTU 10 MW reference Wind Turbine, Progress report Report-I-0092, DTU Wind Energy (2013).

[44] G. Newaz, M. Mayeed, A. Rasul, Characterization of balsa wood mechanical properties required for continuum damage mechanics analysis, Proceedings of the Institution of Mechanical Engineers, Part L: Journal of Materials: Design and Applications 230 (1) (2016) 206–218.

[45] W. W, Mechanical behaviour of composite sandwich panels in bending after impact, MS Thesis, University of Twente.,Enschede, Netherlands (2016).

[46] M. Vural, G. Ravichandran, Microstructural aspects and modeling of failure in naturally occurring porous composites, Mechanics of Materials 35.

[47] M. Borrega, L. J. Gibson, Mechanics of balsa (Ochroma pyramidale) wood, Mechanics of Materials 84 (2015) 75–90.

[48] P. U. Haselbach, K. Branner, Initiation of trailing edge failure in full-scale wind turbine blade test, Engineering Fracture Mechanics 162 (2016) 136–154.

[49] V. Tagarielli, V. Deshpande, N. Fleck, C. Chen, A constitutive model for transversely isotropic foams, and its application to the indentation of balsa wood, International Journal of Mechanical Sciences 47 (4-5) (2005) 666–686.

[50] A. Workbench, et al., Ansys inc, Canonsburg, PA. Ver 12.

[51] H. B. Dhia, Multiscale mechanical problems: the arlequin method, Comptes Rendus de l'Academie des Sciences Series IIB Mechanics Physics Astronomy 12 (326) (1998) 899–904.

[52] S. Xiao, T. Belytschko, A bridging domain method for coupling continua with molecular dynamics, Computer methods in applied mechanics and engineering 193 (17-20) (2004) 1645–1669.

[53] J. Fish, R. Guttal, The s-version of finite element method for laminated composites, International Journal for Numerical Methods in Engineering 39 (21) (1996) 3641–3662.

[54] H. Hu, S. Belouettar, M. Potier-Ferry, et al., Multi-scale modelling of sandwich structures using the arlequin method part i: Linear modelling, Finite Elements in Analysis and Design 45 (1) (2008) 37–51.

[55] Q. He, H. Hu, S. Belouettar, G. Guinta, K. Yu, Y. Liu, F. Biscani, E. Carrera, M. Potier-Ferry, Multi-scale modelling of sandwich structures using hierarchical kinematics, Composite Structures 93 (9) (2011) 2375–2383.